Analysis of steel wire rope mesh as roof support in underground mines

RJ Smith

orcid.org/ 0000-0002-4708-5318

Dissertation accepted in fulfilment of the requirements for the degree *Master of Engineering in Mechanical Engineering* at the North-West University

Supervisor: Dr F Moyo

Graduation: August 2024

ABSTRACT

Fatalities in underground mines due to rockfalls have significantly decreased since 1993. This is due to the improvement in underground roof support technologies, including wire mesh screens. Mine Support Products (MSP) designed and manufacture their own wire mesh made of galvanized steel wire rope. The aim of this study was to analyse the mechanical behaviour of MSP's wire mesh when subjected to an impact load.

Four configurations of the wire mesh with different diameter and construction wire ropes were tested using the drop test. Drop tests were done with a 455 kg weight from various heights and the wire mesh deflection was measured afterwards. The four different configurations chosen was made of 3 mm (7x7), 5 mm (7x7) and 4 mm (1x19) wire ropes weaved in a certain pattern to form a wire rope mesh. From the drop tests it was evident that the 4 mm (1x19) inner and outer wire rope mesh performed the best. No fracture of the wire ropes occurred after a drop test height of 300 mm and the wire mesh deflection therefore still within spec. The other three configurations also performed within specification by not deflecting more than 400 mm from a drop test height of 100 mm. Therefore, MSP's wire meshes are suitable for use as roof support in underground mines.

Finite Element Analysis (FEA) of the drop tests was done on three different configuration wire meshes and compared with experimental results. FEA software Ansys LS-DYNA was used. FEA of drop tests were done on the 3 mm (7x7) inner 5 mm (7x7) outer wire rope mesh, 3 mm (7x7) inner 4 mm (1x19) outer wire rope mesh and the 4 mm (1x19) inner and outer wire rope mesh. The FEA drop test results showed a good correlation with experimental results, with deflection differences between the two methods ranging from 1.1% to 18%. Von mises stress analysis also revealed that the highest stress was at the mesh attachment points. This corresponded with experimental results where fracture of wire ropes occurred at the attachment points.

The corrosion behaviour of MSP's wire mesh was also analysed. Salt spray tests were done on galvanized, bitumen coated and PVC coated wire ropes. Bitumen and PVC coated wire ropes had noticeable corrosion resistance when compared to uncoated galvanized wire ropes. Galvanized wire ropes were also left in an underground gold mine for 76 days. Following this exposure, tensile tests were carried out on the corroded wire ropes and compared with the breaking strength of uncorroded wire ropes. Tensile tests revealed that the corroded wire ropes had breaking strengths 22.5% lower than their uncorroded counterparts. Therefore, corrosion had a noticeable effect on the wire rope breaking strength.

Keywords: Steel wire rope mesh, impact analysis, underground mining roof support

TABLE OF CONTENTS

LIST OF TABLES

LIST OF FIGURES

CHAPTER 1 INTRODUCTION

1.1 Background

Fatalities in South African underground mines have decreased significantly since 1999. There has been a 76% decrease in fatalities between 1999 and 2021 (Minerals Council South Africa, 2021); 51 fatalities were recorded in 2019, the lowest in the history of South African mining, even though the number of employees has risen since 1999. Most fatalities were caused by rockfalls. Rockfalls are caused by seismic events, blasting, drilling, exposure of the rock to moisture and air, or changes in rock stress (Iramina *et al.*, 2014) . Fatalities due to rockfalls have decreased by 85% since 1993 (Minerals Council South Africa, 2019). This is primarily due to improvement in underground mining roof support technologies including wire mesh screens.

Screen material in the form of welded or galvanized chain link steel wire mesh reinforced with steel wire ropes are mostly used for underground roof support (Figure 1). Galvanized chain link mesh is formed by bending individual wires to form diamond shaped apertures (Figure 2 (a)). Welded mesh is made by welding individual wires to form a wire mesh screen as shown in Figure 2 (b). Wire mesh screens are installed to protect people and equipment from small pieces of rocks falling in between rock bolts. These screens thus form a critical part of underground mine roof support. Welded and galvanized chain link steel wire mesh designs have proven to be quite cost-effective whilst still meeting the necessary kinetic energy requirements. However, according to the Harmony Gold standard operating procedure for temporary and permanent netting installation (Harmony Gold, 2020), they require an overlap of two apertures between mesh screens to provide sufficient support. This equates to a maximum of 300 mm overlap, contributing to total material cost. Harmony Gold is one of South Africa's largest gold mines and operates nine underground mines in the country (Harmony Gold, 2023).

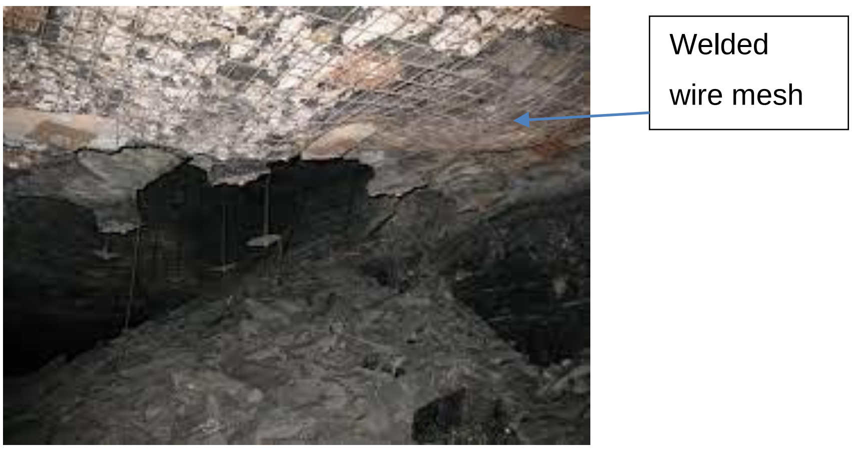

Figure 1: Welded wire mesh installed underground

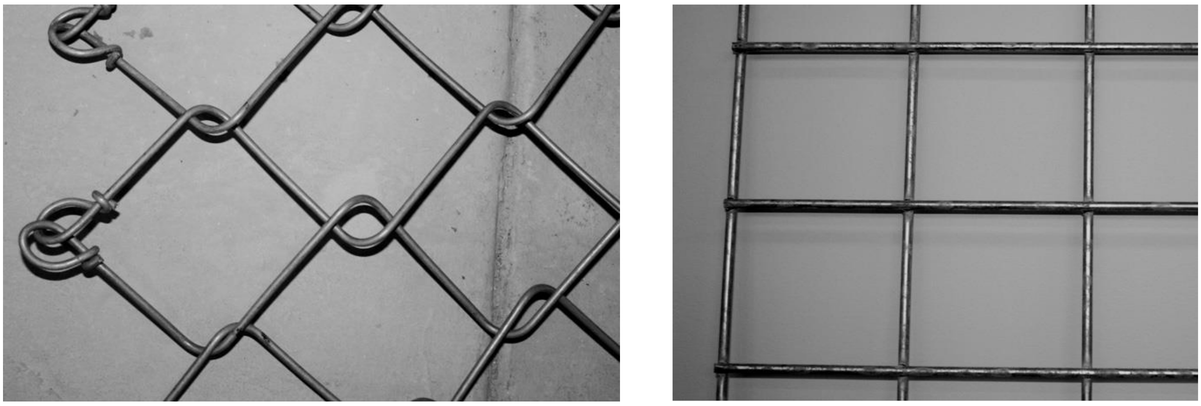

(a) (b)

Figure 2: (a) Chain link and (b) welded wire mesh typically used in underground mine roof support (Player *et al*., 2008)

During application, wire meshes are typically fixed on the mine roof at 1.5 m intervals. Washer plates, S-hooks and U-hooks attached to rockbolts and mechanical jacks are the most common surface fixtures. Mechanical jacks are used to jack wire meshes up to the mine roof with compressive forces of 25 – 30 kN. These surface fixtures are important to minimise deflection of wire meshes and conform to the specific mining maximum allowable deflection. For example, Harmony Gold which produces 42 tons of gold per year in South Africa, has a standard task procedure that requires a 450 kg weight to be stopped by a wire mesh with maximum allowable central deflection of 400 mm (Harmony Gold, 2016). If the wire mesh deflection is excessive, as shown in Figure 3, it may cause harm to people and equipment. The procedure also specifies that the drop test height has to be 100 mm and the 1.5 x 1.5 m mesh must be attached at four attachment points.

Figure 3: Chain link wire mesh deflection after fall of ground

Mine Support Products (MSP) situated in Vereeniging, South Africa, entered the underground mining wire mesh market in 2021 by designing and patenting a wire mesh for use in mine permanent roof support. The wire mesh, made of galvanized steel wire rope coated with bitumen, could be more cost-effective than wire meshes used in most South African mines, including Harmony Gold. At Harmony Gold, an overlap of 300 mm between wire meshes is required in all directions as per their standard task procedure for all temporary and permanent wire mesh installations (Harmony Gold, 2020). An overlap less than 300 mm poses a safety risk as loose rocks may fall in between wire meshes and cause harm to people and equipment. MSP's patented wire meshes, however, form a modular system (Figure 4 (a)) by connecting individual wire meshes with Rocnet connectors as shown in Figure 4(b), which prevents the wire mesh modular system from failing at the intersections. Both the inner and perimeter wire ropes are inserted into the Rocnet connectors to ensure adequate support at connection points. Thus, no overlap is required as can be seen in Figure 5(a). This means that for an area of 40.5 m^2 covered by MSP's wire mesh, only 32.76 m^2 is covered by competitor wire meshes of a similar size due to the 300 mm overlap, which equates to a 20% material saving.

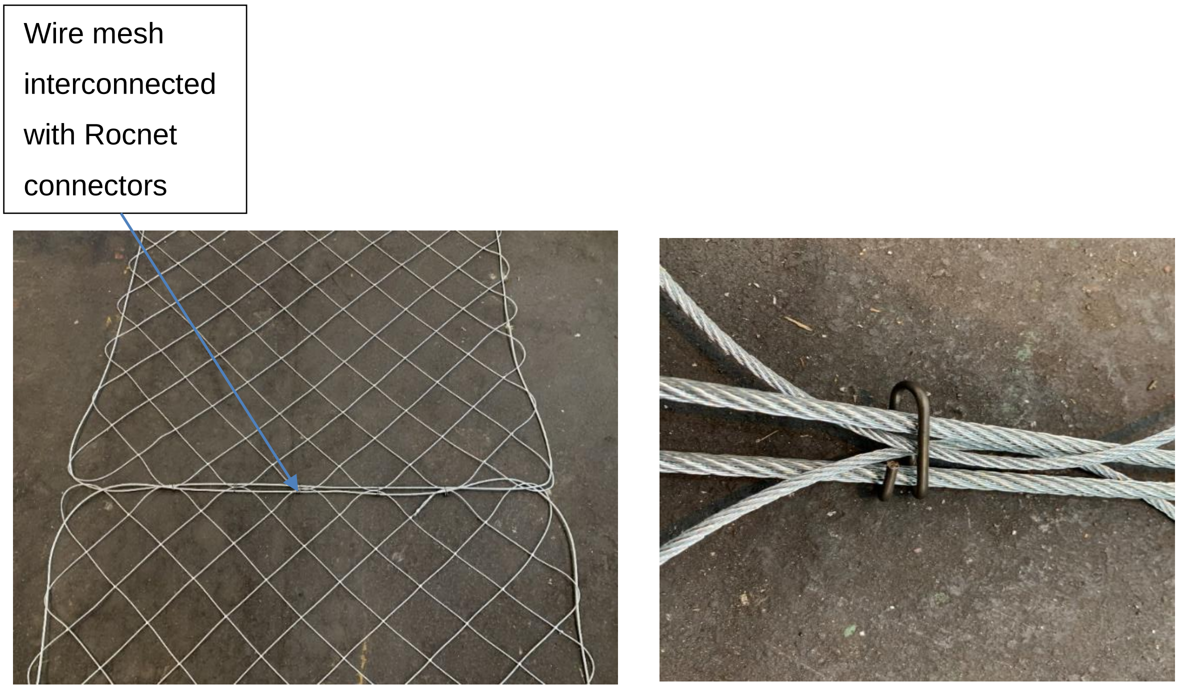

(a) (b)

Figure 4: (a) Wire mesh modular system, and (b) Rocnet connector

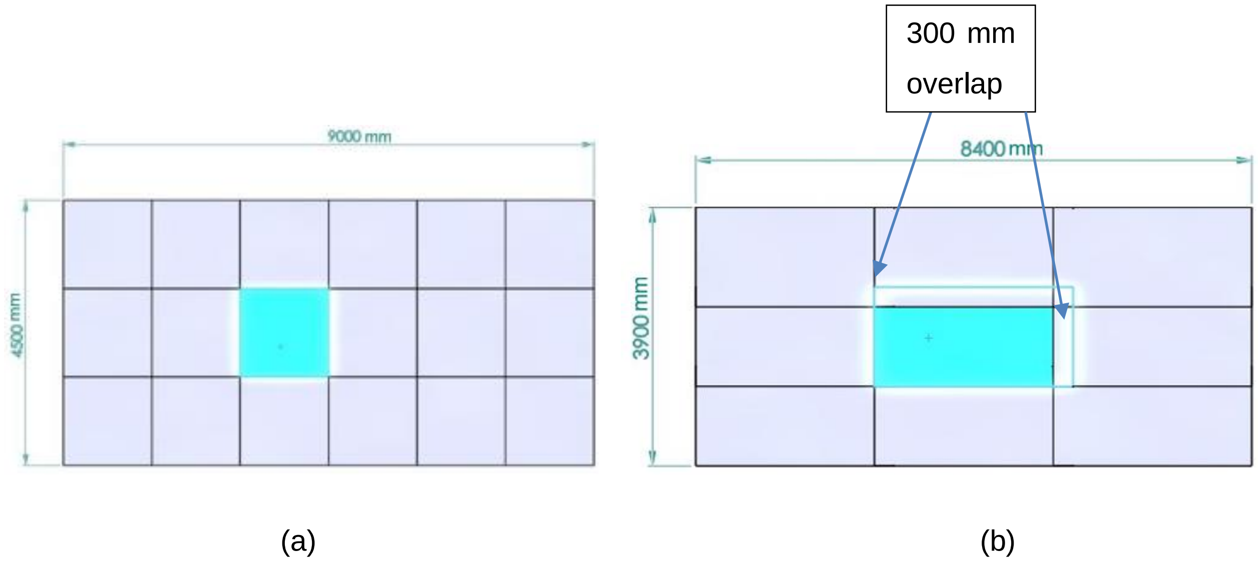

Figure 5: (a) MSP wire mesh modular system, and (b) competitor's modular system with overlap

Table 1 compares prices of the competitor's 5 mm chain link wire mesh and MSP's wire mesh, both currently in use at Harmony Gold. From Table 1 it is evident that MSP's wire mesh is R67.67 cheaper per m^2 (van der Westhuizen, 2020). When accounting for the 300 mm overlap needed by MSP's competitor, the 20% material saving by MSP's wire mesh is R111.00 per m^2 cheaper. MSP's wire mesh will thus be financially beneficial for the company and its customers.

Table 1: MSP vs competitor wire mesh price comparison

	MSP wire mesh	**Competitor wire mesh**	**Competitor wire mesh with 20% extra material**
Price per m^2	R149.00	R216.67	R260.00

1.2 Problem statement

MSP designed and are currently manufacturing and selling a patented wire mesh made of galvanized steel wire rope, which is also coated with bitumen to improve corrosion resistance. MSP's wire mesh has been used by Harmony Gold as mine roof support since January 2021. An example of the wire mesh is shown in Figure 5(a) and 6(a). The wire mesh is 1.5 x 1.5 m, and consists of an inner cable and perimeter cable. The inside cable is weaved diagonally and clamped at each intersection with mild steel clevis clips (Figure 6(b)).

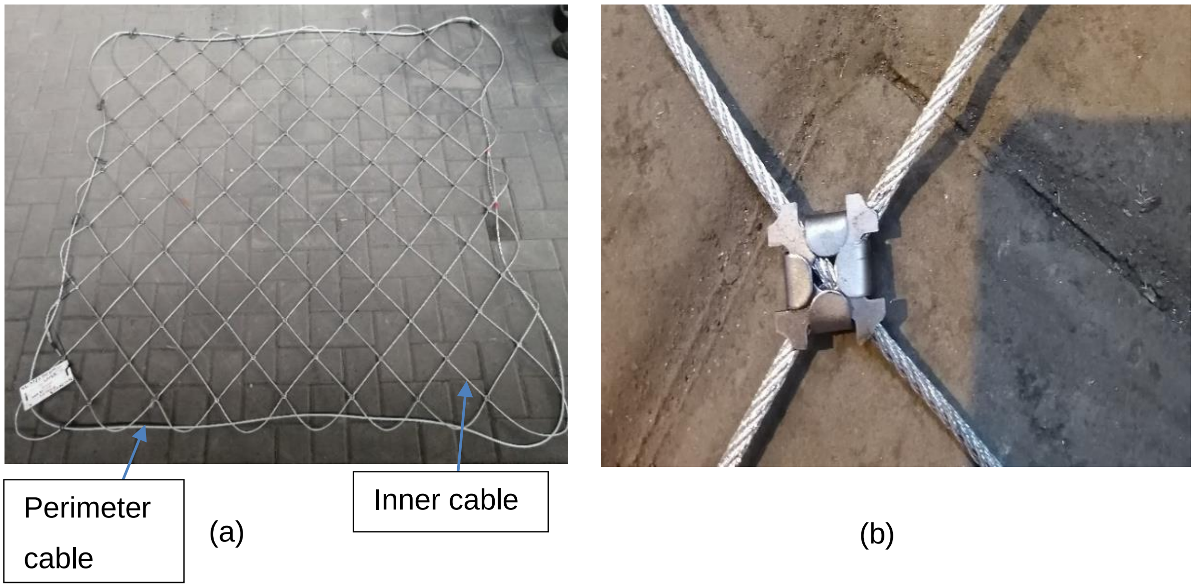

Figure 6: MSP's wire mesh (a) manufactured mesh, and (b) clevis clips at each inner cable intersection

The diagonally weaved inner cable forms 150 x 150 mm apertures. The perimeter cable is weaved around the perimeter of the wire mesh over and under each loop of the inner cable to provide additional support to the inner cable. Mild steel clevis clips consist of a top and bottom part with the cable clamped in between. Clamping the top part by bending it prevents the cables from moving during application.

As illustrated in Table 1, MSP's wire mesh could be a cost-effective alternative to competitor meshes in use in most mines, however its mechanical behaviour under impact loading is unknown. MSP thus needs scientific validation on the behaviour under impact loading of the wire mesh they are currently selling. Failure of the wire mesh could result in reputational and economic damage to the company. This might thus have a negative impact on future ventures into the market for the company. Scientifically validating MSP's wire mesh will also give the company the opportunity to use scientific reports as a marketing tool to send to customers and potentially expand its market share. Since the wire mesh modular system is a novel and patented solution, there remains a knowledge gap that needs to be addressed experimentally.

1.3 Aim and objectives

The aim of this project is to study the mechanical behaviour of MSP's wire mesh when subjected to an impact load.

The objectives of the study are:

1. To determine and compare the breaking strength and stiffness of different diameter and construction wire ropes using tensile tests.

2. To determine and compare the displacement and peak force of different configurations of MSP’s wire mesh under impact loading using the drop test.

3. To perform Finite Element Analysis (FEA) of the displacement of the wire mesh when subjected to the drop test and compare the results with experimental drop test data.

4. To determine the influence of corrosion on MSP’s wire mesh in an underground mining environment and under accelerated corrosion conditions.

1.4 Dissertation structure

Chapter 1: Introduction

An introduction to the dissertation. The improvements in mining safety and shortcomings of current mine roof support meshes are discussed. The problem statement and aim and objectives are also given in this chapter.

Chapter 2 Literature review

The literature from previous studies related to the objectives of this paper is surveyed in this chapter.

Chapter 3 Methods

The method for the manufacturing of the wire mesh is discussed in this chapter. The procedures for drop tests, FEA and influence of corrosion on the galvanized wire rope are also specified.

Chapter 4 Results and discussion

New wire ropes are tested to determine their breaking strength. Drop tests and FEA’s on different configuration wire meshes are done thereafter. Experimental and FEA drop test results from the three different configurations wire rope meshes are presented and compared. Additionally, the influence of corrosion on galvanized wire ropes is also discussed.

Chapter 5 Conclusions and recommendations

Conclusion of the dissertation. Evaluation on whether the aims and objectives of the study were achieved. Recommendations for future studies are also discussed.

CHAPTER 2 LITERATURE REVIEW

2.1 Introduction

This chapter details the literature survey of existing research on various underground mine roof support meshes, including welded and chain link mesh, polymer mesh and steel-plastic geogrid. The boundary conditions and their influence on drop test results are discussed. Finite element analysis of welded and chain link wire mesh, as well as stainless steel woven wire mesh, is examined and analysed. The influence of corrosion on galvanized steel and steel wire ropes in underground mining environments is analysed. Additionally, accelerated corrosion tests of galvanized steel and steel wire ropes are evaluated.

2.2 Welded and chain link mesh

A study was done by Player *et al.* (2008) on two of the most widely used type of wire meshes in underground mining. One wire mesh was made of galvanized high tensile steel wires and the other was made of welded steel wires. Galvanized steel comprises a protective layer of zinc for corrosion protection. High tensile steel wires has a tensile strength of 1860 MPa which means smaller diameter wires could be used when compared to mild steel wires with a tensile strength of 550 MPa (Du *et al*., 2018). Reducing the wire diameter results in a lighter wire mesh, which could help with more efficient installations underground. This reduced installation time for roof support can contribute to increased mine productivity.

The galvanized wire mesh screen was made of 4 mm diameter steel wires woven together in a zigzag pattern to form a diamond-shaped grid (Player *et al.*, 2008). The woven steel wires form a chain link, which ensures the diamond-shaped grid is of a fixed shape (Figure 2(a)). The welded wire mesh screen comprised 5.6 mm steel wires that were welded together to form a square grid pattern (Figure 2(b)). Tag welds ensure the square grid is of a fixed shape. The chain link and welded wire mesh screens were installed on a rigid frame and restrained along each of its sides instead of only at four corners; this setup is called rigid boundary conditions. Boundary conditions are the corners where the wire meshes are fixed when installed (Player *et al.*, 2008).

In both the static and drop tests the chain link mesh had a higher breaking strength than the welded wire mesh (Player *et al.*, 2008). Static tests were conducted at a constant speed of 4 mm per minute. The static breaking strength of the welded wire mesh was 44 kN, while that of the chain link wire mesh was 145 kN. Similar observations were made by Schoevaerts *et al*. (2012) in static tests, where a 4 mm diameter chain link wire mesh fractured at 110 kN. The displacement of the welded mesh at failure was 170 mm while that of the chain link mesh at the same load was 180 mm, which indicates a slightly better stiffness of the welded mesh under static load (Player *et al.*, 2008). Failures of the welded wire mesh included ductile fracture of the steel wire and brittle fracture at the weld heat affected zone (HAZ), as shown in Figure 7. Ductile fracture takes place when a material undergoes significant plastic deformation before fracturing, whereas brittle fracture occurs more rapidly with little to no plastic deformation (Jiqin, 2018). Brittle fracture can thus occur with little or no warning signs.

The HAZ is the material next to the welding that is not melted but has undergone changes in its microstructure due to exposure of high temperatures during the welding process. A change in microstructure causes a change in mechanical properties of the material. For example, in a study done by Adedayo *et al*. (2010), mild steel plates were arc welded and analysis of the heat affected zone revealed finer grains often linked with rapid cooling. Tensile stress, yield stress and hardness were also higher closer to the fusion line and gradually decreased further from the weld. Thus, brittle failure of the welded mesh may be caused by the increased hardness of the steel wires in the HAZ. The chain link wire mesh failure was caused by the edges of the loading plate cutting the wires of the wire mesh (Player *et al.*, 2008). A similar failure of the chain link wire mesh was observed by Schoevaerts *et al*. (2012). However, no further static tests were done to assess the performance of the mesh without the loading plate cutting the wires. Smoothening the edges of the loading plate should eliminate this failure mechanism wherein the loading plate cuts the wires.

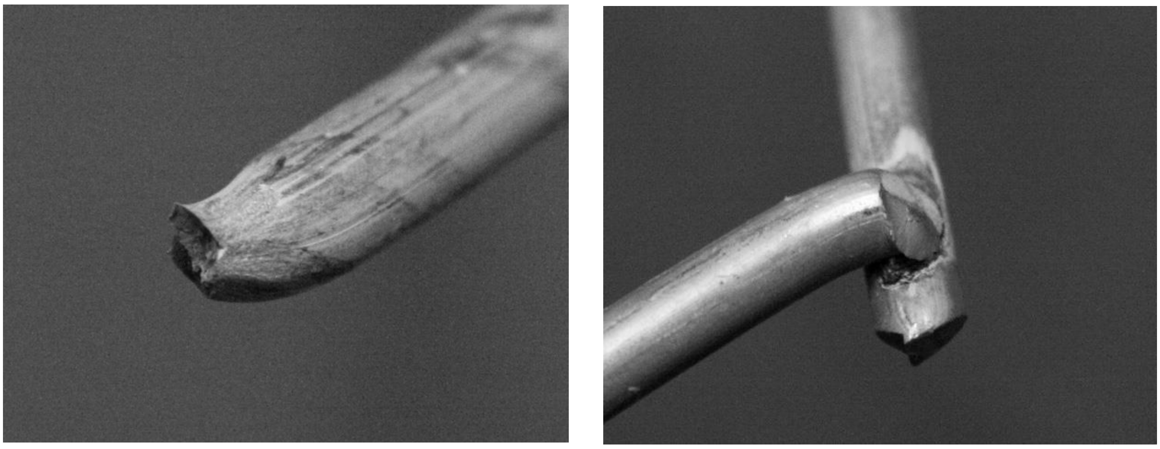

(a) (b)

Figure 7: (a) Welded wire mesh ductile fracture and (b) brittle fracture at the heat affected zone (Player *et al*., 2008)

For the drop test, the welded wire mesh failed at an average kinetic energy of 2 kJ, which equates to a breaking strength of 55 kN. For the chain link mesh the average kinetic energy at failure was 9 kJ, which equates to a breaking strength of 185 kN. The displacement of the welded wire mesh at failure was 203 mm, while the chain link mesh, under the same load, reached 215 mm of displacement. This indicates that the welded wire mesh had slightly higher stiffness when subjected to dynamic loading. As with the static test, the drop test failure mechanism of the welded wire mesh was also due to ductile fracture of the steel wire and brittle fracture at the weld heat-affected zone. The chain link mesh failed at the links between the wires due to ductile fracture. Failure at the links between the wires may be due to strain hardening of the wires changing its mechanical properties and decreasing ductility. During strain hardening of steel, its yield strength increases but ductility decreases (Dubina *et al*., 2004). This is due to increase in dislocation density, and thus increased resistance to deformation.

The static force at failure of the welded wire mesh was 25 % more than the dynamic force at failure, while that of the chain link mesh was 27.6 % more. From this comparison it is evident that static tests cannot accurately predict how meshes would behave under dynamic loading conditions, such as those that may occur during a fall of ground in an underground mine.

Although the welded steel wires had a bigger diameter, they failed at a lower kinetic energy than the smaller diameter chain link wire mesh due to brittle fracture at the HAZ. The welded mesh deflected slightly less than the chain link mesh. This could be due to plastic deformation of the links of the chain link mesh when subjected to static or dynamic loads. Less deflection may be preferred in lower stoping widths due to the proximity of the employees to the mine roof. Stoping width refers to the height of the mine roof. However, the difference in deflection between the chain link and welded mesh under dynamic loads was only 5.9 %.

Instead of tag welds or chain links, the inner cable of MSP's wire mesh is clamped with clevis clips. The clevis clips prevent the wire ropes from moving and does not change the microstructure of the wires through welding or bending. The bending flexibility of wire ropes prevents plastic deformation during the weaving process in the manufacturing of the wire rope mesh, which also ensures no changes of the wire microstructure. Unlike the tests done on the chain link and welded mesh which were clamped along each side, MSP's wire mesh will be connected to four boundary conditions for a 1.5 x 1.5 m mesh size as per Harmony Gold standards. The boundary conditions are determined by the temporary and permanent roof support spacings and may vary from one mine to another.

2.3 Polymer mesh

Polymer materials are also used to form mesh for underground roof support (Skarbøvig *et al*., 2011). Three types of mesh configurations used are braids, webbing, and twisted vines. Braids, made of high density polyethylene (HDPE), are the most common type of mesh used for the inner mesh, ranging in diameter from 4 mm to 8 mm. Different materials are used for the inner braids, perimeter, and mesh reinforcement ropes (Figure 8). Perimeter and reinforcement ropes, ranging from 10 mm to 12 mm in diameter, are used as support for the inner braids and are made of polyester and polypropylene. Reinforcement ropes play a vital role in transferring the load from the inner mesh to the attachment points of the net.

HDPE, polypropylene and polyester have very low water absorption rates of 0.01% (Grishanov, 2011; Guo *et al*., 2019). Due to the high humidity of underground mines, mechanical properties of materials with low water absorption rates remain mostly unaffected. These materials have low susceptibility to corrosion in underground mining conditions; however, abrasion wear of the rope fibres may occur during the handling of the mesh, which may affect its performance.

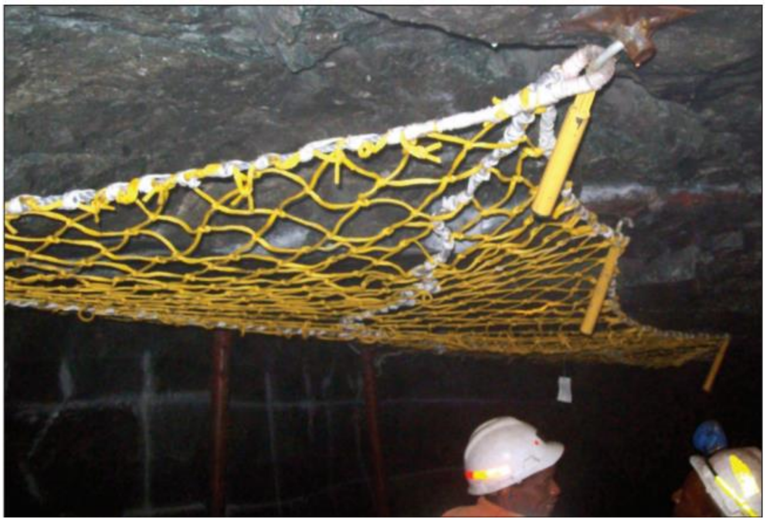

Figure 8: Polymer mesh (Skarbøvig *et al*., 2011)

Diamond and square orientation meshes were drop tested to compare their maximum energy absorption and deflection (Skarbøvig *et al*., 2011). Diamond mesh refers to the inner mesh being at 45° angle to the perimeter rope while the square orientation is parallel to the perimeter rope. Diamond meshes were found to fail at an average kinetic energy of 3.53 kJ, with the square counterparts at 2.21 kJ. Diamond meshes transferred the load from drop tests more effectively to the boundary anchor points, while the square orientation mesh transferred the load mainly to the perimeter rope as illustrated in Figure 9. Diamond mesh orientation thus allows more of the load to be transferred through the inner mesh along its diagonal strands. In contrast, the square orientation mesh may require a perimeter rope with higher tensile stress because its design does not efficiently transfer the load through the inner mesh. The two mesh orientations had similar deflections from different drop heights. Therefore, diamond orientation mesh is the preferred choice due to its superior performance, and it uses approximately the same amount of material as square orientation mesh.

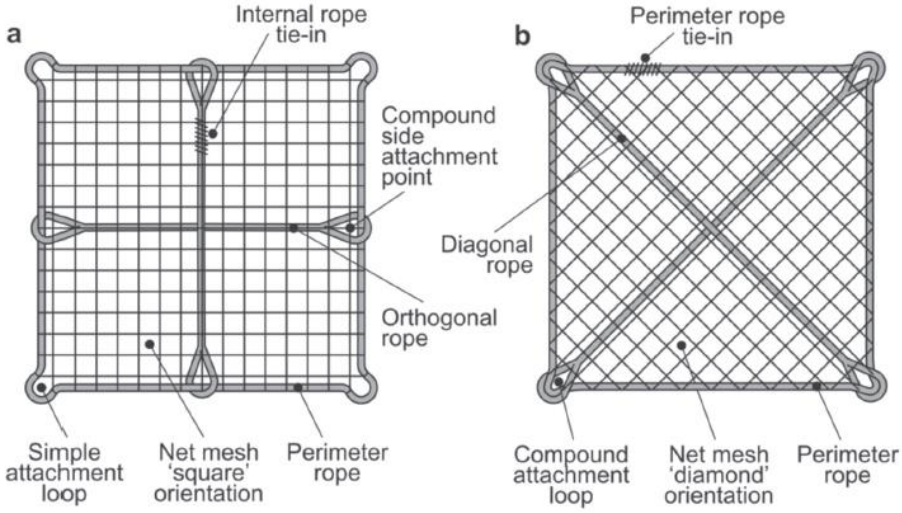

Figure 9: (a) Square and (b) diamond orientation mesh (Skarbøvig *et al*., 2011)

Figure 10: Polymer mesh after drop test (Skarbøvig *et al*., 2011)

A comparison was also made between polymer meshes with and without perimeter and reinforcement ropes (Skarbøvig *et al*., 2011). The mesh without perimeter ropes failed at a kinetic energy of 2.21 kJ with 700 mm deflection, while the mesh with perimeter ropes failed at a kinetic energy of 3.97 kJ and 750 mm deflection. Adding diagonal reinforcement ropes further increased the kinetic energy at failure to 4.86 kJ and 720 mm deflection. This observation was supported in a study done by Potvin and Heal, (2010). Welded mesh with 5.6 mm diameter wire was reinforced with 12.7 mm diameter perimeter and diagonal wire ropes (Figure 11), which increased the maximum static load from 4 tons to 15 tons. These improvements in deflection, maximum kinetic energy and maximum static load may be attributed to the loads being transferred from the inner mesh to the perimeter and reinforcement ropes which are connected to the mesh attachment points.

Figure 11: Welded mesh reinforced with wire rope (Potvin and Heal, 2010)

The energy absorption capability of welded mesh reinforced with wire rope can be further increased by controlling the torque applied to nuts of Crosby clamps. Ferrules or Crosby clamps are used to connect two endpoints of wire ropes (Figure 12). Controlling the torque applied to the nuts of the Crosby clamps allows for more deflection of the wire rope, which prevents it from fracturing (Ortlepp & Stacey, 1997). A similar approach of using friction clamps to allow wire ropes to slide at a certain load was followed by Duffy (1992). Ferrules are used to connect the endpoints of MSP's wire ropes because they are more cost effective and more practical to use during manufacturing.

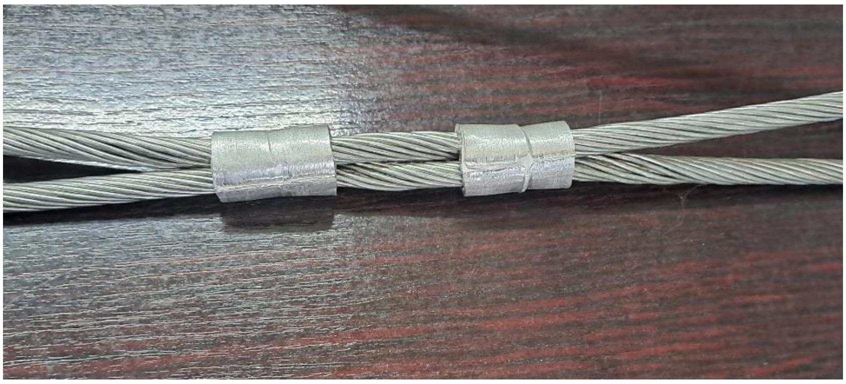

Figure 12: Ferrules used to connect two endpoints of wire ropes

Braid mesh with reinforcement and diagonal ropes were installed underground to determine the ease of installation (Skarbøvig *et al.*, 2011). Three different anchor points namely C-hooks, S-hooks and mechanical jacks clamping the net to the hanging wall were used. The hanging wall is the mine roof above where the ore is present. Clamping the mesh to the hanging wall with mechanical jacks was found to be the most common and easiest way of surface fixture (Figure 13). These surface fixtures were found to be acceptable as long as they did not damage the mesh. Depending on the mine practice and standards, plates attached to rockbolts are also widely used as surface fixtures (Whiting, 2017).

Figure 13: Mechanical jacks used to clamp braided mesh to the hanging wall (Skarbøvig *et al*., 2011)

2.4 Steel-plastic geogrid

Wang *et al*., (2022) investigated steel-plastic geogrid possibly replacing conventional wire meshes for underground roof support. Following the completion of static tests on geogrids and tensile tests on individual geogrid members, underground testing was conducted at Xiaogou mine in China. Geogrids were made of extruded high strength steel wires wrapped with high strength polyethylene, the nodes were then molded together by injection bonding to form a geogrid mesh. Polyethylene wrapping of the steel wires serves as corrosion protection. Increasing the strands inside the polyethylene wrap increased the strand and geogrid strength.

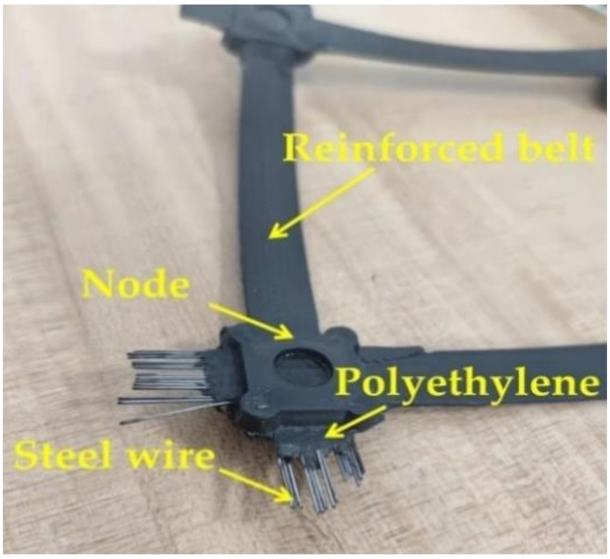

Figure 14: Steel-plastic geogrid composition (Wang *et al*., 2022)

The injection molded node points were tested and the results compared well with the welded joints on welded mesh (Wang *et al*., 2022). Four and 6 mm diameter welded mesh were used, while 10, 14 and 16 wires with diameters of 0.7 mm each were used for geogrid members. For both meshes the failure of welded joints and molded node points was substantially lower than the breaking strength of the welded mesh wire and geogrid strands. Breaking strength is the maximum tensile force at the breaking point of a test piece (Saville, 1999). This indicates that the welded joints may fracture, and the molded nodal points may peel before fracture of the steel wires occurs. Failure at the welded joints was also observed during static and dynamic testing of 5.6 mm diameter welded wire mesh by Player *et al*. (2008).

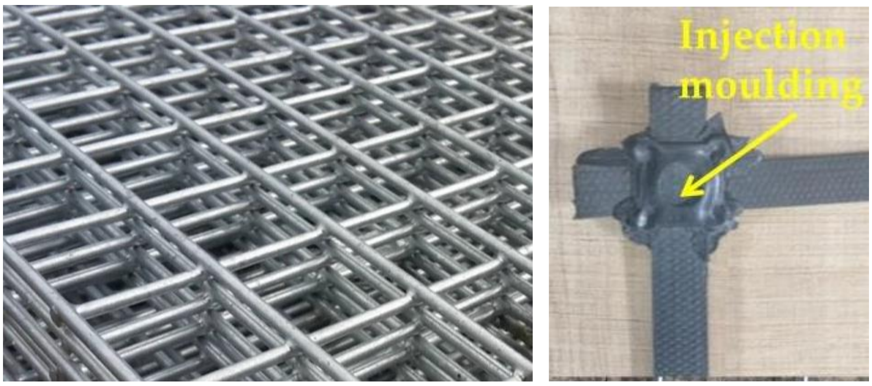

(a) (b)

Figure 15: (a) Welded wire mesh and (b) injection bonded geogrid nodes (Wang *et al*., 2022)

Static tests were also done on 800 x 800 mm steel-plastic geogrid and welded wire mesh samples (Wang *et al*., 2022). Once again, the steel-plastic geogrid compared well with the welded steel wire mesh. However, there were no impact tests done on the steel-plastic geogrid to analyse its behaviour under impact load.

Both steel-plastic geogrid and welded steel wire mesh samples were clamped along each side, which is not practically feasible in underground installations. Attachment points in underground installations are determined by rockbolt spacings according to mine procedures, as shown in Figure 16. For example, the Harmony Gold standard operating procedure for temporary and permanent netting installation. Clamping the mesh along each side distributes the force more uniformly through the mesh. Using only four anchor points as per Harmony Gold mine procedure would concentrate the force from falling rocks on the mesh attachment points. The distance between mesh attachment points are determined by permanent and temporary roof support spacing. These supports include mechanical jacks, hydraulic props, mechanical props and rockbolts. The specific support spacing varies with mines and is determined by factors such as the type of supports used, the mining method in use and prevailing rock conditions (Braczak, 2005). In the case of Harmony Gold, the testing configuration for mesh attachment points consists of four attachment points for 1.5 x 1.5 m mesh and six attachment points for 1.5 x 3 m mesh (Harmony Gold, 2016).

Welded wire mesh and geogrid mesh were also compared in underground tests (Wang *et al*., 2022). The geogrid mesh was easier to install thus reducing the labour costs. Due to the irregular shape of the rock face, the deformation capacity of the geogrid mesh is an advantage as it fits better to the surrounding rock (Figure 16). Corrosion of the welded mesh was also observed while the geogrid was corrosion free. However, the exposure period for both meshes was not specified in the study.

Figure 16: Welded wire mesh vs geogrid mesh underground installation (Wang *et al*., 2022)

2.5 Rigid versus laced boundaries

A comparative static test was done on laced (Figure 17(a)) versus rigid boundary conditions (Figure 17(b)) by Morton *et al.* (2007). Boundary conditions are the points where the mesh is attached to the test frame. In underground installation it is the points where the mesh is attached to S-hooks, U-hooks, rockbolts or clamped to the hanging wall with mechanical jacks. It was found that laced boundary conditions affect the total displacement of the mesh before fracture. This was primarily a result of the wire ropes tensioning after the test has started, leading to more displacement occuring before the mesh started to take load. As a result, some kinetic energy may have been transferred to the lacing. Rigid boundary conditions with mild steel eye nuts and shackles were used for drop tests on MSP's wire mesh. Rigid boundary conditions are the best method for transferring all the kinetic energy from the drop test to the wire mesh, and these are also the boundary conditions used in underground mining.

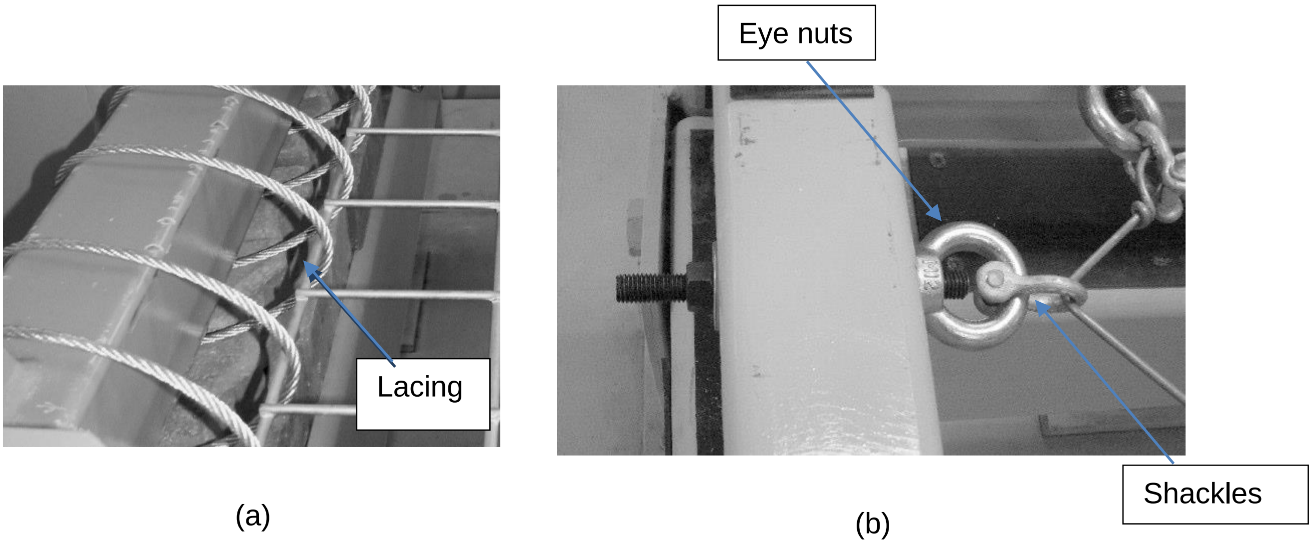

(a) (b)

Figure 17: (a) Laced boundary condition and (b) rigid boundary condition (Morton *et al*., 2007)

Static tests on welded wire mesh with different boundary conditions were also done by Dolinar (2006). Two different size bearing plates were used as attachment points namely 152.4 x 152.4 mm and 203.2 x 203.2 mm (Figure 18). The influence of different bolt torques on wire slippage was also evaluated. Wider bearing plates had a significant impact on improving the peak loads and stiffness of the mesh due to a larger area being covered. Increasing the bolt torque also increased the mesh stiffness and peak load.

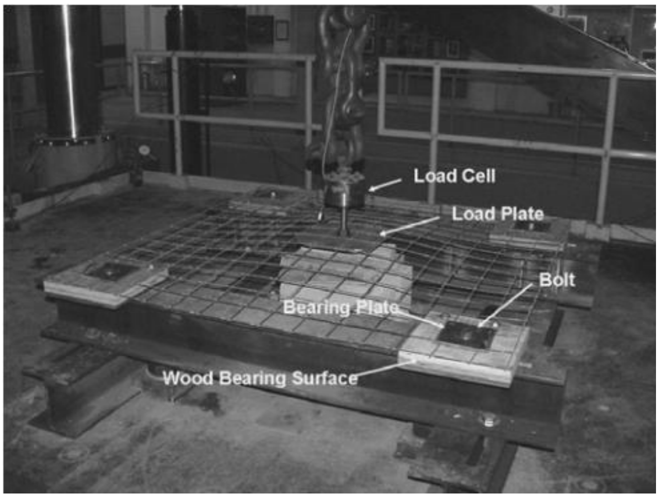

Figure 18: Test setup with bearing plates used as attachment points (Dolinar, 2006)

2.6 Finite Element Analysis of wire mesh

2.6.1 Welded and chain link wire mesh

Three dimensional non-linear modelling was done on a static force applied on chain link wire meshes (Morton *et al.*, 2007). Finite Element Analysis (FEA) software FARO and rigid boundary conditions along each side of the mesh were used. FARO was designed for dynamic impacts but can also be used for static loads of constant velocity. Boundary conditions along each side of the mesh distribute the force more uniformly along the wire mesh. From the FEA static load that was applied, the deflection was 7% more than the experimental results, indicating a good correlation between the two. FEA's of drop tests were also done on FARO on ring meshes which compared well with experimental results (Volkwein, 2009). It was therefore found that using three dimensional non-linear modelling software FARO is an accurate way of predicting the force-displacement graph for wire meshes subjected to a static and dynamic loads.

2.6.2 Stainless steel woven wire mesh

Numerical and experimental results of low velocity impact tests on warp and weft woven stainless steel wire meshes were compared by Wang *et al.* (2021). Warp and weft wires are terms used in textile weaving, in which the lengthwise warp wires are held in tension while the transverse weft wires are drawn through and weaved over and under the warp wires as shown in Figure 19. These meshes are used as security screens for doors and windows and therefore should be able to witstand high impact during forced breakage.

Impact tests were done on 250 x 150 mm samples at the centre of the mesh and samples were clamped along two sides. The Instron CEAST 9350 drop weight impact test facility was used for these tests. Impact energies ranged from 25 to 100 J. Due to the smaller samples of 250 x 150 mm used and the mesh application as a security screen, these impact energies are not comparable with the requirements of Harmony Gold. However, this study helps to evaluate how FEA drop tests on wire meshes compares to experimental results.

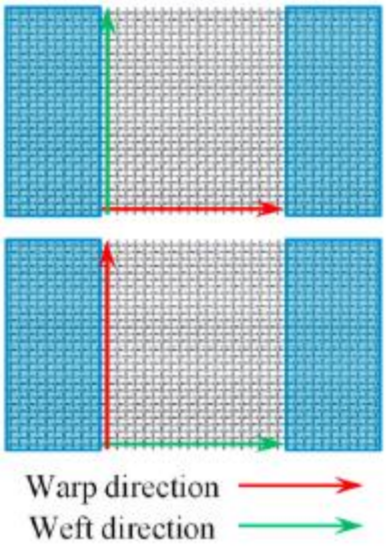

Figure 19: Warp and weft directions (Wang *et al.*, 2021)

FEA software ANSYS/LS-DYNA was used to obtain numerical results and compare with experimental results (Wang *et al.*, 2021). Each wire was meshed using solid elements. 12 mesh elements along the wire's wavelength and 28 along its cross section were chosen (Wang *et al.*, 2021). Results are more accurate when more mesh elements are used, however computing time increases. The correct balance between computing time and accuracy must thus be determined. As per the experimental tests, two sides of the mesh were fixed. The impactor was defined as a solid element, thus assuming negligible elastic deformation. The density was adjusted to obtain the mass used in the experimental test.

Contact between the impactor and mesh was defined as Automatic Surface to Surface (Wang *et al.*, 2021). Ls Dyna Automatic Surface to Surface function automates the process of checking for penetration within the master and slave nodes. The master is the fixed part with defined boundary conditions while the slave is the moving part.

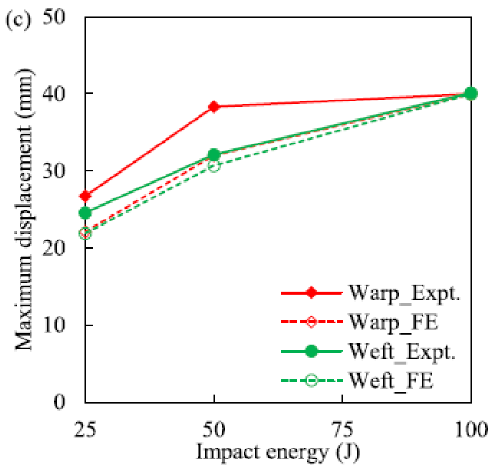

Figure 20: Comparison of experimental and FEA results under different impact energies (Wang *et al*., 2021)

The FEA results for force-displacement graphs and energy absorbed correlated well with experimental results (Figure 20). At an impact energy of 25 J the difference between experimental and FEA displacement was 15% for the warp wire and 8% for the weft wire. At 50 J, these differences were 18% for the warp wire and 6% for the weft wire. At 100 J there was essentially no difference in displacement between the experimental and FEA results. ANSYS/LS-Dyna can thus be used to predict the mechanical behaviour of wire meshes when subjected to impact loading from drop tests. A similar FEA setup may be selected for MSP's wire mesh due to the similarities of the drop tests.

2.7 Influence of corrosion on wire ropes

2.7.1 Corrosion in underground mining environments

Wire ropes have applications in various industries including mining, construction and engineering and typically consist of steel wires braided around a central steel wire core as illustrated in Figure 21. Braiding the steel wires in this arrangement allows it to be more elastic while still having high tensile strength. Wire ropes may be made of steel, stainless steel, galvanized steel, and bronze of which galvanized steel is the most popular. Often, wire ropes and other carbon steel are coated with PVC to provide an additional layer of protection against corrosion (Bandeira *et al*., 2017). In this study, the focus will be on galvanized steel wire ropes, the material used in MSP's steel wire mesh. Additionally, the corrosion resistance of bitumen coatings will also be analysed, which is what MSP's wire mesh is coated with. The corrosion resistance of PVC coated wire ropes will also be examined.

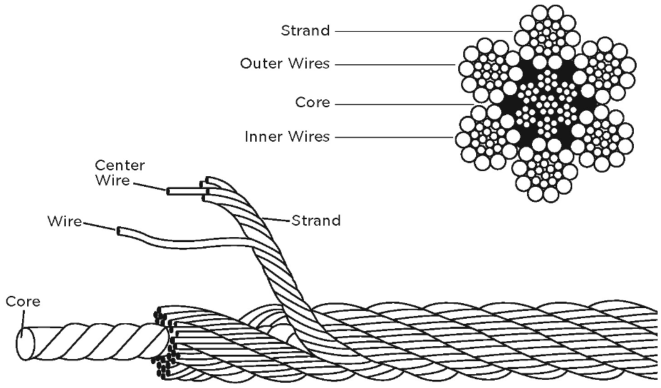

Figure 21: Wire rope core arrangement (Miami Stainless, 2020)

A comparison was made between steel and galvanized steel coupons installed in 5 underground mines in Canada (Dorion *et al*., 2009). The relative humidity of the mines ranged from 58% to 96% and the temperatures from 11.5 to 29.3°C. It was found that the corrosion rate of coupons left in groundwater was more than those left in atmospheric conditions. Corrosion rates typically increase above a relative humidity of 60% and double with an increase of 10°C in temperature (Dorion *et al.*, 2009). This observation was also made in a study done by Suzumura and Nakamura (2004).

Chemical analysis of the groundwater revealed the presence of ions such as SO_4^- and Cl^-. SO_4^- and Cl^- are aggressive ions that can attack the surface of metals (Dorion *et al*., 2009). Corrosion rates were lower for galvanized steel coupons than the steel coupons due to the protective layer of zinc on the galvanized coupons. It was also found that over time solid mineral deposits formed on steel and lowered the corrosion rate (Dorion *et al.*, 2009). A similar observation was also made by Fayyad *et al*. (2024) where carbon steel was covered with FeS_2 and SiO_2 deposits to determine the effect on its corrosion resistance. After 24h in an electrolyte solution, the FeS_2 and SiO_2 deposits decreased the corrosion rate of the bare metal by 18.3 and 3.1 times respectively.

Hadjigeorgiou et al., (2008) also did a study on the corrosion of underground mine support systems in different underground mine sites in Canada. Wire mesh and rock bolts were exposed to underground environments for periods ranging from 3 to 180 months. Visual observations of the degree of corrosion were made, ranging from localized corrosion after 18 months of exposure to advanced corrosion after 180 months. Galvanized wire mesh was more resistant to corrosion than ungalvanized support systems. Chloride and sulphate ions in water are aggressive and were found in high concentrations in two of the mine sites. The support systems in one of these sites experienced localized corrosion to advanced corrosion after just 3 months of exposure, which may be attributed to the high concentrations of sulphate. Additionally, the high relative humidity of 90 to 100% may have further accelerated the corrosion rate, although temperature was lower at 15 to 19°C.

Two case studies were also done on the fracture of steel wire ropes in two different Indian coal mines (Singh *et al.*, 2016). In the first case study the fracture of a 25 mm diameter 6 x 10 fibre core arrangement winding steel wire rope, which was used in the hoist system of a drill rig, was examined. In the second case study a 32 mm diameter 6 x 7 fibre core arrangement steel wire rope used as a guide rope was analysed. The wire rope core arrangement is the arrangement in which individual wires are constructed (Figure 21).

In the first study, examination of a failed galvanized steel wire rope revealed evidence of stress corrosion cracking (SCC) (Singh *et al.*, 2016). SCC occurs when a crack slowly and progressively grows under stress within an environment susceptible to corrosion and failure occurs below the yield stress of the material (Chen *et al.*, 2022). SCC and abrasion wear were contributing factors in the reduction of the wire rope diameter by 58%. This reduction in diameter may thus cause the wire ropes to fail by fatigue and fracture. Fatigue failure of multiple wires may have caused the tensile overload and ductile fracture of the remaining wires (Zhang *et al*., 2017). Fatigue occurred due to cyclic loading during operation of the hoisting system. A reduction in the wire rope diameter may cause it to fail at a lower load than that of a new wire rope, which might cause it to fail prematurely when subjected to dynamic or static loads.

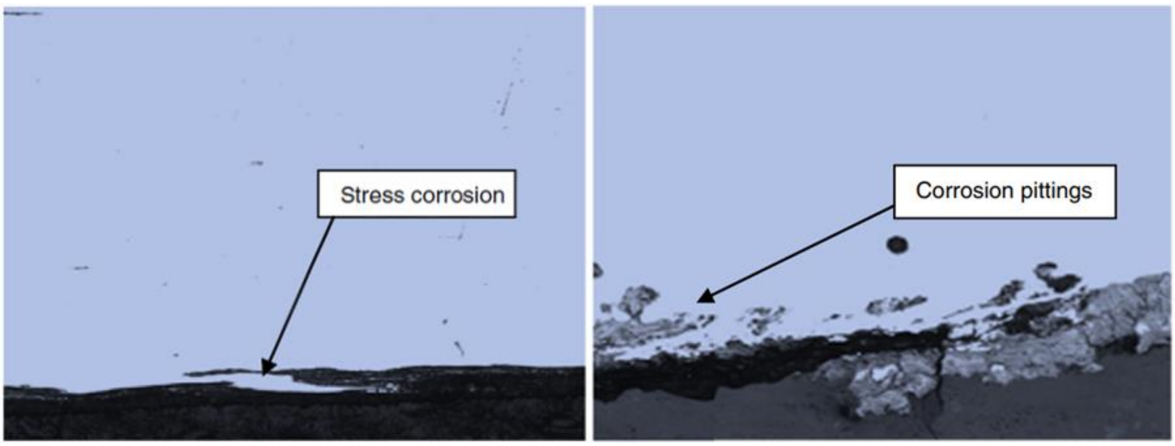

Figure 22: Micro examination of the failed wire rope revealing Stress Corrosion Cracking and pitting corrosion (Singh *et al*., 2016)

In the second study intergranular corrosion, pitting and uniform corrosion were observed on the non-galvanized steel wire rope (Singh *et al.*, 2016). Intergranular corrosion occurs along the grain boundary, with the grain mostly unaffected. Pitting corrosion forms pits in the metal (Figure 22) and may cause SCC and perforation (Burstein *et al.*, 2004). Pits that formed due to pitting corrosion also cause stress concentration in the material. Therefore, through the combination of localized pitting corrosion and applied stress, cracks may be initiated and propagate in the material, leading to SCC. Uniform corrosion results in the uniform loss of metal. Intergranular corrosion, pitting corrosion, uniform corrosion and a distorted grain were all contributing factors in the fracture of the wire ropes. Grains start to distort during plastic deformation of the material (Keran *et al*., 2017). Grains that have been over distorted can result in the development of residual stresses.

Poor lubrication of the wire rope may also have resulted in abrasion making it more prone to corrosion (Singh *et al.*, 2016). As the extent of corrosion increases, the coefficient of friction between individual wires also increases. Adequate lubrication may increase the wear resistance of steel wire ropes, subsequently reducing corrosion. A similar observation was also made by Huang *et al*. (2023). It is therefore evident that corrosion of wire ropes due to mining underground conditions could cause it to fail at loads lower than design loads. A lower breaking strength may affect the maximum static and dynamic loads of the wire mesh.

Groundwater may also affect the corrosion of steel in underground mines. In a study done by Fortes *et al*., (2022), the effect of acid mine drainage on carbon steel was investigated. Acid mine drainage is a process that results from mining processes, leading to the formation of sulfuric acid, dissolved iron, and the precipitation of ferric hydroxide. The sulfuric acid dissolves metal elements from mining, infiltrates into the ground and ultimately contaminates the groundwater (Iatan, 2021).

Thirty carbon steel metal plates with dimensions 50 x 60 x 6 mm were kept in water contaminated with acid mine drainage (Fortes *et al*., 2022). The tests were conducted for thirty weeks, and one plate was taken from the water solution every week. Each metal plate was then dried, and its weight measured to determine the mass loss. It was found that the water solution greatly affected the weight and thickness of the metal plates with decrease in mass and thickness each week (Figure 23). After 30 weeks the metal plates basically disappeared. Thus, it is evident that metal immersed in groundwater and contaminated by acid mine drainage experiences substantial loss in cross sectional area, consequently affecting its strength.

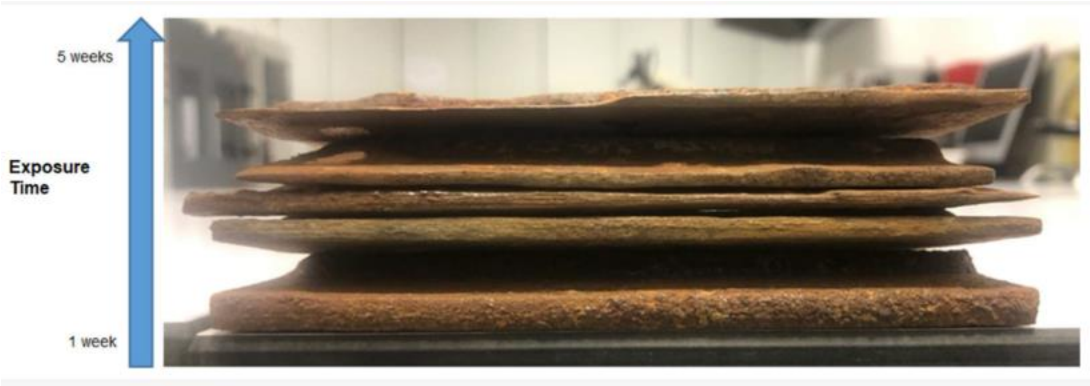

Figure 23: Thickness loss of carbon steel test specimens (Fortes *et al*., 2022)

2.7.2 Accelerated corrosion tests

Accelerated corrosion tests were done on galvanized steel wire ropes used as suspension bridge cables (Suzumura & Nakamura, 2004). Four tests with different conditions were conducted. In the first test the wires were constantly wet (specimen S). The second test (specimen U) involved subjecting the wires to cycles of wet and dry conditions. In the third test (specimen L), the wires were fully immersed in water. Finally, the fourth test (specimen C) maintained a constant relative humidity of 100%. The effect of temperature on corrosion rate was also tested in intervals of 10°C, ranging from 10 to 40°C. It was found that the mass loss increased linearly with time and increase in temperature and was highest at 40°C (Figure 24). Tests on these four specimens were therefore conducted at 40°C.

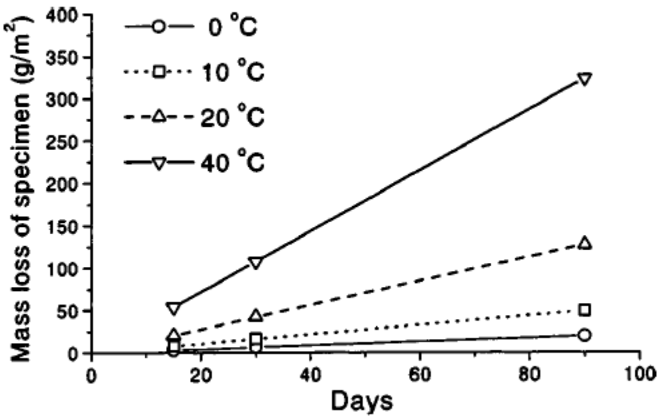

Figure 24: Influence of temperature on corrosion rate of galvanized steel wire rope for specimen S (Suzumura & Nakamura, 2004)

Specimens were taken out of the enclosed box and their mass loss were calculated. Specimens S exhibited signs of brown corrosion products, although no pitting corrosion was observed. Specimen L showed signs of dark grey corrosion products, while specimens U and C displayed white corrosion products. These grey and white corrosion products are indicative of the corrosion of the zinc layer, with the steel unaffected. Corrosion of zinc occurs when moisture is present on its surface. The presence of moisture acts as a solvent for atmospheric elements and a medium for electrochemical reactions, which cause hydroxide to form (de la Fuente *et al*., 2007). The mass loss of these four specimens is shown in Figure 25.

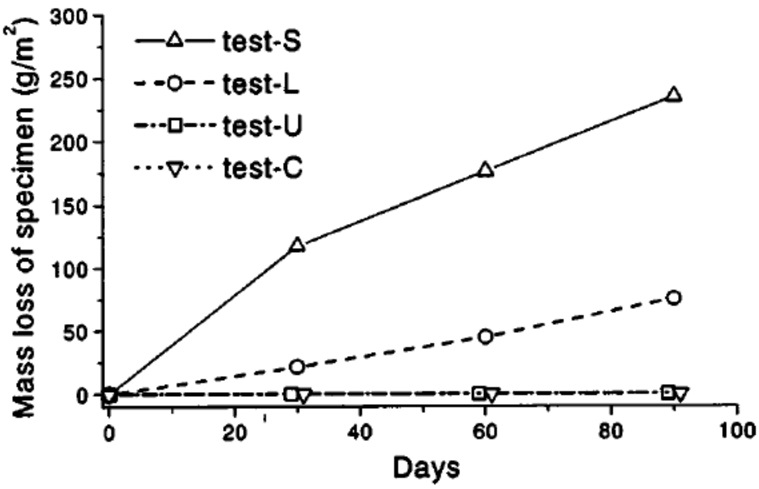

Figure 25: Corrosion rate of specimens (Suzumura & Nakamura, 2004)

It was clear that specimen S exhibited the highest level of corrosion due to its continuous exposure to wet conditions. Despite the minimal mass loss observed in specimens U and C, the relative humidity of 100% still led to the formation of white corrosion products (Suzumura & Nakamura, 2004).

Tests were also conducted to determine the effect of sodium chloride on corrosion rates of suspension bridge cables (Suzumura & Nakamura, 2004). Sodium chloride concentrations may vary depending on different atmospheric conditions but has been found to be about an average of 0.1 g/m^2 in suspension bridge cables. This may however increase in rare cases, which can accelerate corrosion rates even further. For the three tests sodium chloride concentrations of 0, 0.1 and 10 g/m^2 were thus used. Specimens were kept constantly wet as this is when corrosion is most severe. The results of these tests are given in Figure 26.

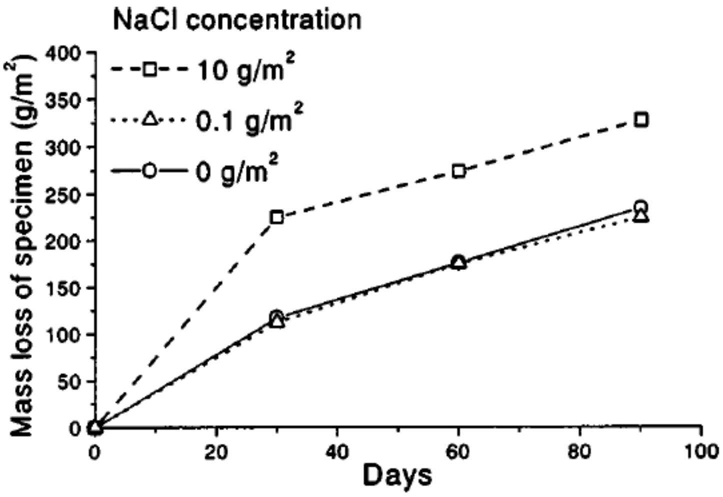

Figure 26: Mass loss of specimens kept constantly wet while containing different levels of sodium chloride (Suzumura & Nakamura, 2004)

From Figure 26 it is evident that an increase in sodium chloride causes an increase in corrosion. An increase in temperature also caused an increase in corrosion (Figure 24). In a study done by Brownlie *et al*. (2022), the influence of NaCl concentration on the corrosion rates of low alloy steel was also analysed. Concentrations of 0.05 wt% NaCl, 3.5 wt% NaCl and 10 wt% NaCl were used. Corrosion rates peaked at 3.5 wt% NaCl and decreased at 10 wt% NaCl. This may be due to the amount of dissolved oxygen decreasing at higher concentrations of NaCl. The higher concentration NaCl caused lower solubility of oxygen in the NaCl solution. Therefore, higher corrosion rates were noted in a moderately concentrated sodium chloride solution, while a decrease was observed in solutions with higher concentrations of sodium chloride.

Accelerated corrosion tests, of which salt spray testing is the most common, are often used to analyse the influence of corrosion on materials. Unlike tests conducted in the real environment, salt spray tests greatly shorten test time. In a study done by Zhao *et al*. (2023), salt spray tests were done on galvanized steel wire with maximum exposure time of 510 h. The test was conducted in a salt fog test chamber. The test temperature of 35°C, NaCl concentration of 50 g/L and the spray solution ph of 6.5-7.2 were maintained throughout. After 264 h of exposure the galvanized steel wire showed traces of white corrosion products, after 384 h minimal brown corrosion spots appeared and after 510 h a lot of brown red corrosion was evident. Pitting corrosion of the steel wire was visible after the corrosion products were removed.

Corrosion of steel wires can generally be divided into two phases. Initially, corrosion affects the coated surface, and once the corrosion is deeper than the coating thickness it starts penetrating the steel wire. The salt pray test was thus a good indication of the corrosion resistance of a galvanized steel wire.

Bitumen coating of steel is a cost effective way of improving its corrosion protection. Bitumen does not have inherent corrosion resistance properties, it creates a protective layer that prevents corrosion agents from reaching the metal surface (Guma *et al*., 2015). Bitumen is usually heated to 150 to 250°C to achieve a viscosity low enough for it to be applied to metal surface. Application methods include dipping, spraying, mopping and rolling. The most common forms of bitumen used in the coating industry are asphalt and coal tar. Coal tar is more effective than asphalt in moisture resistance, which makes it more suitable for corrosion protection in underground mines (Hayes, 1940). Applying a bitumen coating to MSP's wire rope serves as a cost-effective method to provide an additional layer of corrosion protection. Bitumen is also readily available, and the coating process is integrated into MSP’s wire mesh manufacturing process by means of dipping or spraying.

Aluminium-zinc coatings have also been used to further increase the corrosion resistance of steel wires. In a study done by Miyachi *et al*. (2013), the corrosion resistance of steel wires coated with Al-Zn was compared with Zn-coated wires. Accelerated corrosion tests were conducted with the steel wires kept in different corrosion conditions namely: at a relative humidity of 60%, a relative humidity of 100% and constantly wet. The temperature was kept constant at 40°C and the test was conducted over a period of 5 months. Suzumura and Nakamura (2004) observed that mass loss due to corrosion increases linearly with time and is highest at 40°C. The mass loss due to corrosion of the Al-Zn coated wires was much less than that of the Zn coated wires (Miyachi *et al*., 2013). Al-Zn coatings of wire ropes may thus be a viable way of improving its corrosion resistance. However, integrating this technology into the manufacturing process of suppliers, especially for smaller diameter wire ropes such as those used in MSP's wire mesh, may pose some challenges.

2.8 Chapter summary

Different types of wire mesh were analysed. Welded and chain link wire meshes, which are the most used in underground mines, showed good results in both experimental static and dynamic tests. In all tests the meshes were attached to anchor points along each side. Similarly, in FEA drop tests, wire meshes were attached to anchor points along each side. This highlights the need for experimental and FEA dynamic tests, specifically drop tests, with wire meshes attached at only four points as per the Harmony Gold standard.

Various studies have also examined the corrosion of steel wire rope and galvanized steel. These include accelerated corrosion tests such as salt spray testing on galvanized steel wire, investigations into the effects of varying concentrations of sodium chloride on galvanized steel wires, and analyses of the impact of different temperatures and atmospheric conditions on galvanized steel wires. However, not much has been done on the corrosion resistance of bitumen-coated galvanized wire ropes, similar to those used in MSP's wire mesh.

CHAPTER 3 METHODS

3.1 Introduction

In this chapter, the methods used for the wire mesh manufacturing, wire rope tensile tests, wire mesh drop tests, FEA and corrosion are described. Four different wire mesh configurations for drop testing were manufactured on production tables in accordance with MSP general work instructions. The drop test procedure was developed with the resources available and working within the budget provided by MSP, while also adhering to the Harmony Gold standard (Harmony Gold, 2016). The method followed for tensile testing of wire ropes is also described.

The FEA of the drop test was designed with the resources provided by the North-West University (NWU). The FEA was also developed based on information available from previous studies and designed to replicate the setup of the experimental drop test. The method to determine the influence of corrosion on wire ropes in an underground environment was done with the limited access available to underground mines provided by MSP's sales department. Furthermore, the method for conducting accelerated corrosion tests is described.

3.2 Wire mesh manufacturing

Wire meshes were manufactured at MSP's factory, in Vereeniging South Africa. Meshes were manufactured on a production table as per MSP general work instructions. As can be seen in Figure 27 (a), the galvanized steel wire ropes were weaved in a fixed configuration. The cable ends were tensioned by hand and connected with aluminium ferrules. Ferrules are used to connect two endpoints of wire ropes. Clevis clips were bent and hammered flat at each wire rope intersection (Figure 27 (b)). After manufacture, the wire mesh was dipped in bitumen for an extra layer of corrosion protection.

(a) (b)

Figure 27 : Wire rope mesh weaved in a fixed configuration and (b) clevis clips hammered flat

Four different configuration wire meshes were manufactured and subjected to drop tests, as shown in Table 2. Selection of these configurations considered the availability of cable supply from both local and international suppliers as well as the potential market volumes for wire mesh. Wire ropes with certain constructions are readily available locally while others need to be imported. Importing a significant portion of the wire rope might impact the compliance of the wire rope mesh with the mining charter, which stipulates a minimum of 60% local content for manufactured mining goods (Department of Mineral Resources, 2018). It was also chosen to save project costs as inner steel wire ropes with a diameter bigger than 4 mm would require manufacturing of larger clevis clips. Using larger clevis clips would necessitate the production of new dies for the forming process, as well as an increased amount of material. Similarly, if wire ropes larger than 6 mm are used, it would be necessary to manufacture larger Rocnet connectors which would increase MSP's wire mesh cost.

Table 2: Wire mesh cable configurations

Configuration Number	**Inner cable specifications**		**Perimeter cable specifications**	
	Diameter (mm)	**Core arrangement**	**Diameter (mm)**	**Core arrangement**
1	3	7 x 7	5	7 x 7
2	3	7 x 7	4	1 x 19
3	4	1 x 19	4	1 x 19
4	3 (Wire mesh modular system)	7 x 7	5 (Wire mesh modular system)	7 x 7

The wire mesh cable configuration is the configuration of inner and perimeter cables used for three different configuration wire meshes. Configuration 4 consisted of two 1.5 x 1.5 m meshes hooked together with six Rocnet connectors to form a 1.5 x 3 m wire mesh modular system (Figure 4). Using six Rocnet connectors ensures that there is a connector at every loop of the mesh, except at the attachment points to the frame. This helps reduce confusion regarding connector spacings in underground installations.

MSP currently manufactures its wire meshes using 5 mm (7 x 7) outer and 3 mm (7 x 7) inner wire ropes. Different wire mesh configurations, as outlined in Table 2, were manufactured and tested to determine their performance in comparison to the original design. Alternative option wire mesh configurations would allow MSP to use different wire ropes in case of supply issues.

3.3 Tensile tests

Tensile tests were done on 3 mm (7 x 7), 4 mm (1 x 19) and 5 mm (7 x 7) diameter wire ropes to determine their breaking strength. Tensile testing the 4 mm (1 x 19) wire rope would determine if it could be used as an alternative to the 3 mm and 5 mm wire ropes in the event of limited supply. The 4 mm wire rope may be a more economically viable option due to its simpler 1 x 19 construction. Cheaper wire rope would reduce the overall cost of MSP's wire mesh, making it a more cost effective product.

A stress-strain graph was also created to compare the tensile strength and stiffness of the different wire ropes. Stress was calculated using Equation 1:

$$\sigma = \frac{F}{A} \tag{1}$$

Where σ is the stress, F the force and A the cross sectional area of the tested specimen. The strain was calculated using Equation 2:

$$\varepsilon = \frac{\Delta L}{L} \tag{2}$$

Where ΔL is the change in length of the specimen and L is its original length.

Tensile tests were done at Vaal Metallurgical Laboratory as per tensile testing of metallic materials standard ISO 6892-1 (ISO, 2019). Tensile tests of corroded 3 mm (1 x 19) galvanized steel wire ropes were also done at Vaal Metallurgical Laboratory to determine the loss of tensile strength due to corrosion. Samples of 150 – 200 mm in length were clamped on each side and tensile tested using a 300 kN Sans universal tensile testing machine (Figure 28) until fracture. As per standard ISO 6892-1, the strain rate was kept between 0.00025 and 0.0025 s^{-1}.

Figure 28: Sans universal tensile testing machine used in the tensile tests

3.4 Drop tests

Drop tests were done at MSP's testing facility in Vereeniging on wire meshes manufactured using different steel wire rope configurations as described in Section 3.2. The test facility consists of a rigid I beam structure as shown in Figure 29.

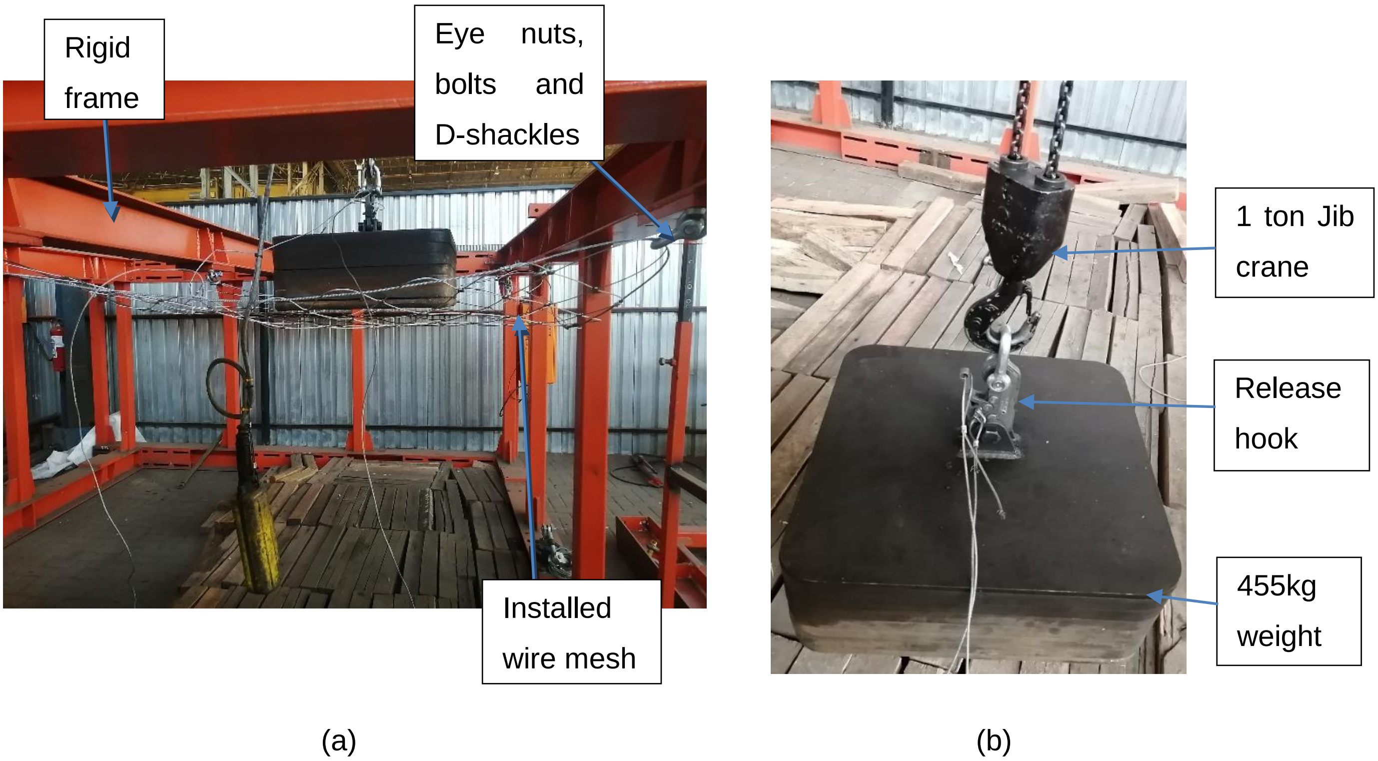

Figure 29: (a) Rigid test frame, and (b) drop test weight attached to release hook and jib crane

The design of the I beam structure consists of I beams bolted together and welded to square tubes, which ensures there is no deflection in the structure and therefore all the kinetic energy from the drop test is transferred to the wire mesh. The I beam structure can be adjusted to exactly 1.5 x 1.5 m as per Harmony Gold mine specifications. Additionally, the wire mesh modular system of 1.5 x 3 m can be accommodated in the test frame.

The Harmony Gold safety netting technical specifications require a 450 kg weight measuring 0.55 x 0.55 m to be used for drop tests (Harmony Gold, 2016). The weight consisted of six 0.55 x 0.55 x 0.03 m mild steel plates which are bolted together. The actual mass of the weight used in this study was found to be 455 kg, which is 1.1% more than the Harmony Gold specification and therefore complies with the requirement. The weight was attached to a mechanical release hook which was hooked to a 1 ton Jib crane (Figure 29 (b)). Due to the unstable electricity grid, a mechanical release hook was used instead of an electromagnet.

The mesh boundary restraints consisted of four corners with D-shackles, bolts and eye nuts, as shown in Figure 29 (a). These boundary restraints ensure that all the kinetic energy from the drop test was transferred to the mesh. The maximum dynamic wire mesh displacement was recorded by an extensometer, and the gravitational force at the centre of the mesh was recorded using an accelerometer. In this study, the terms displacement and deflection of the wire mesh are identical and may be used interchangeably. The data from the accelerometer and extensometer was collected using MatTest software. The g-force from the accelerometer was converted to force using Equation 3:

$$F = mg \tag{3}$$

Where F is the force, m the mass of the weight and g the gravitational acceleration, 9.81 m/s^2. MatTest software recorded the extension and gravitational force every 0.0007 s. The data was exported to Excel and processed further.

The kinetic energy from the drop test was gradually increased by increasing the heights from which the weights were dropped. Drop test heights were increased by increments of 100 mm until the maximum dynamic deflection of the wire meshes were out of the Harmony Gold spec of 400 mm. Increasing the kinetic energy by increasing the drop test height saves project costs as the weight used has a fixed mass. Increasing the mass of the weight would require extra mild steel plates to be manufactured and more time and labour to add or remove these plates.

3.5 Finite Element Analysis

Finite Element Analysis (FEA) of the drop test was done to determine the distribution of stresses in the wire mesh. The von Mises stress criteria was used. Von Mises stress analysis is commonly used to determine the yielding condition of a structure (Yu & Xue, 2022). The FEA was used to complement and supplement the results of the experimental tests. A good correlation in results indicates that FEA can be utilized to identify the failure point of wire meshes, eliminating the necessity to do experimental studies. A good correlation between experimental and FEA results was established by using the accuracy achieved in previous studies as a benchmark. Therefore, conducting FEA's may thus be more cost effective. Force and displacement data were collected and compared to data from the experimental results. This was done on Ansys LS DYNA at NWU Potchefstroom.

Due to the complexity of the wire mesh model, it was created with CAD software Solidworks and imported into Ansys LS DYNA. To simplify the model and decrease the simulation time, the wires were drawn as solid elements instead of individual woven wire ropes. In a study done by Tran *et al*. (2012) on a FEA of a wire rope rockfall protective fence, wire ropes were also modelled as solid wires. The imported wire mesh was auto meshed with an element size of 2.6 mm. This element size was chosen to reduce simulation time, which was already 84 hours for one drop test. Smaller element sizes had a negligible effect on the wire mesh displacement. Boundary conditions of the experimental setup that were defined in Section 3.4 were replicated in the FEA by fixing four corners of the wire rope mesh as shown in Figure 30.

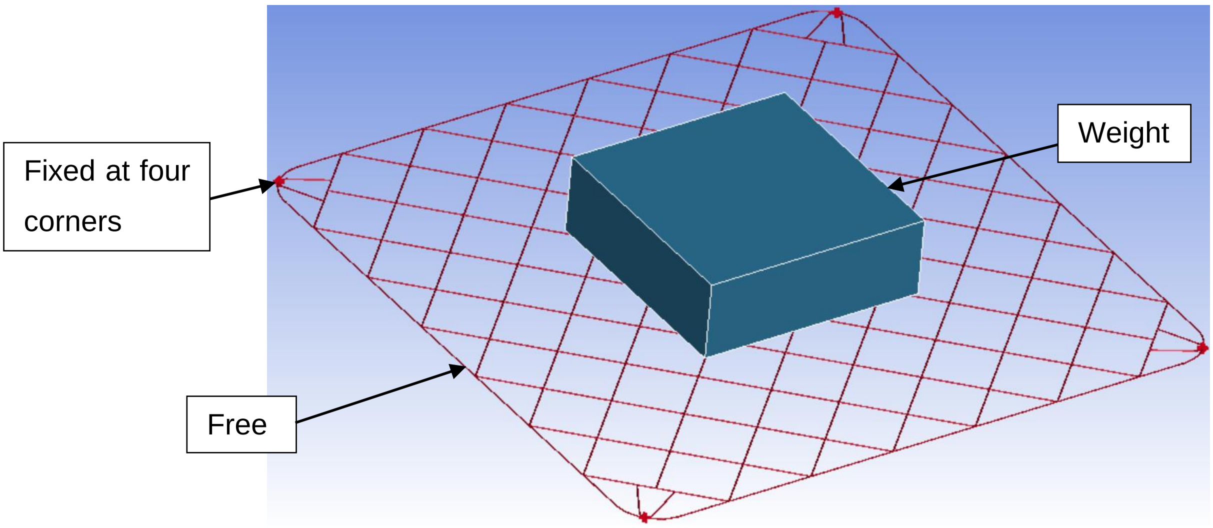

Figure 30: FEA drop test setup with boundary conditions

The imported wire mesh was defined as material mat24–piecewise linear plasticity and a shell element with properties as defined in Table 3. Shell elements give shear deformation and bending properties to a material. Mat24 is an elasto-plastic material, which can also be used for common metals. The deformation of the weight was assumed to be negligible and was therefore defined as a solid element with material mat20-rigid and mechanical properties as defined in Table 3 (Wang *et al.*, 2021). The solid element function is used to model solid structures while mat20 is a material belonging to rigid bodies.

Table 3: Wire rope mesh mechanical properties

	Density (kg/mm^3)	Young's Modulus (GPa)	Poisson's ratio	Yield stress (MPa)
Wire rope mesh	7.8×10^{-6}	210	0.3	550
Weight	7.8×10^{-6}	210	0.3	250

Instead of increasing the drop test height, for each drop test the kinetic energy was increased by increasing the initial velocity, thus decreasing the simulation time. The kinetic energy was calculated using the kinetic energy Equation 4:

$$KE = \frac{1}{2}mv^2 \tag{4}$$

Where KE is the kinetic energy and v the velocity of the weight. The velocity was calculated using Equation 5:

$$v = gt \tag{5}$$

Where t is the time from the point of release of the weight until moment of impact. Time was calculated using Equation 6:

$$t = \sqrt{\left(\frac{2d}{g}\right)} \tag{6}$$

With d being the distance from point of release to point of impact. Using Equations 4, 5, and 6, the initial velocities of the weight dropped from 100 mm, 200 mm, and 300 mm were calculated as 1.40 m/s, 1.98 m/s, and 2.43 m/s, respectively. Interaction between the weight and wire mesh was defined with contact algorithm Automatic Surface to Surface. Automatic Surface to Surface automatically checks shell elements for penetration. The weight was defined as the slave and the wire rope mesh the master. The slave nodes are the nodes that move while the master segment is the part that is stationary. Automatic Surface to Surface contact algorithm checks the nodal displacement at every timestep between entities that are in contact with each other (Wang *et al.*, 2021).

3.6 Influence of corrosion

Galvanized wire ropes were left underground in a South African gold mine in the Free State province and allowed to corrode in-situ. A 3 mm (1 x 19) core arrangement galvanized steel wire rope was used, these wire ropes were not bitumen coated. The wire ropes were left underground for 76 days and placed in the mine stope area. The stope area refers to dugout section and contains the ore that is being mined. The water composition and atmospheric conditions in this area may thus differ compared to other areas. It was also subjected to groundwater generated from the high pressure water system used to collect ore. The atmospheric conditions and water quality of samples were taken from the same South African gold mine where the galvanized wire ropes were left to corrode. This data is given in Table 4.

Table 4: In situ water analysis and atmospheric data

Parameter	units	SA gold mine reading
Depth	m	1400
Temperature	°C	30
Relative humidity	%	95
HCO_3	mg/l	15.25
Ca	mg/l	348.68
Cu	mg/l	0.04
Fe	mg/l	0.01
K	mg/l	177.90
Mg	mg/l	150.20
Na	mg/l	809.97
Zn	mg/l	0.18
Cl	mg/l	2147.56
NO_3	mg/l	163.90
SO_4	mg/l	359.27
pH		7.00

The influence of corrosion on the tensile strength of the corroded steel wire rope was tested as per procedure described in Section 3.3. Tensile tests were done on these galvanized steel wire ropes and compared with non-corroded wire ropes. Hadjigeorgiou *et al*. (2008) conducted a study at the Doyon Gold Mine in Canada, where a similar exposure period of 90 days was applied to welded wire mesh. Subsequently, a visual inspection of the welded wire mesh was performed.

A salt spray test was conducted by Metlab on galvanized, polyvinyl chloride (PVC) and bitumen coated wire ropes. PVC is frequently used in industry to coat wire ropes by means of a wire coating extrusion unit (Cirac & Kozan, 2009). This application of PVC provides an additional layer of corrosion protection to wire ropes and improves abrasion resistance. The salt spray test enables a direct comparison of MSP's bitumen coated wire rope with PVC and galvanized wire ropes. This test was also chosen as the preferred accelerated corrosion test because it is readily available in laboratories in South Africa and it is also commonly used to evaluate the effectiveness of coatings (Baboian, 2007). The wire ropes were subjected to 168 hours of salt spray testing as per ASTM (2018). Sodium chloride was used in a pH range of 6.5 to 7.2. After 168 hours of continuous exposure, the wire ropes were removed from the salt spray chamber and rinsed with distilled water. Photographs of the wire ropes were taken thereafter to report any traces of corrosion.

3.7 Chapter summary

The methodology for this study was developed and presented with consideration given to the conclusions drawn from other relevant studies. The procedure followed for the manufacturing of MSP’s wire mesh was discussed first. Wire meshes were weaved with wire rope in fixed configurations on production tables. Additionally, the procedure followed for tensile testing at Vaal Metallurgical Laboratory was described. These tensile tests will provide the breaking strength of different wire ropes used in the manufacturing of the wire meshes.

A drop test facility was designed and manufactured to conduct drop tests on the different configuration wire meshes. The weight used for these drop tests was manufactured to comply with the Harmony Gold standard (Harmony Gold, 2016). The FEA drop test setup was designed to replicate the experimental drop tests, enabling a comparison of the results between the two tests. The methodology for salt spray testing and corrosion of wire ropes in an underground mining environment was also described.

CHAPTER 4 RESULTS AND DISCUSSION

4.1 Introduction

In this chapter results from tensile tests, drop tests, underground corrosion tests and salt spray tests are presented and analysed. Firstly, tensile tests of 3 mm (7 x 7), 4 mm (1 x 19), 5 mm (7 x 7) and 3 mm (1x19) diameter steel wire ropes are illustrated and compared. The breaking strength and tensile stress of the four different wire ropes are analysed.

Following this, the force and displacement results from drop tests are compared and analysed. The type of wire mesh failures are also examined. Afterwards the displacement from FEA drop tests are presented and compared with experimental results. Additionally, the Von mises stress on the wire mesh is analysed. Lastly, the influence of corrosion on wire ropes from salt spray and underground tests are examined.

4.2 New wire rope tensile tests

Tensile tests were conducted to compare the breaking strength of a 4 mm (1 x 19) diameter wire rope with that of 3 mm (7 x 7) and 5 mm diameter (7 x 7) wire ropes. The objective was to assess the correlation between the breaking strength of wire ropes and the performance of wire meshes. The feasibility of using the 4 mm (1 x 19) wire rope as an alternative option to the 3 mm (7 x 7) and 5 mm diameter (7 x 7) wire ropes currently being used by MSP was also assessed.

The breaking strength of the 3 mm (7 x 7), 3 mm (1 x 19), 4 mm (1 x 19) and 5 mm (7 x 7) wire ropes are compared in Figure 31. The breaking strength of a new 3 mm diameter (1 x 19) wire rope was also tested to compare it with that of a corroded wire rope.

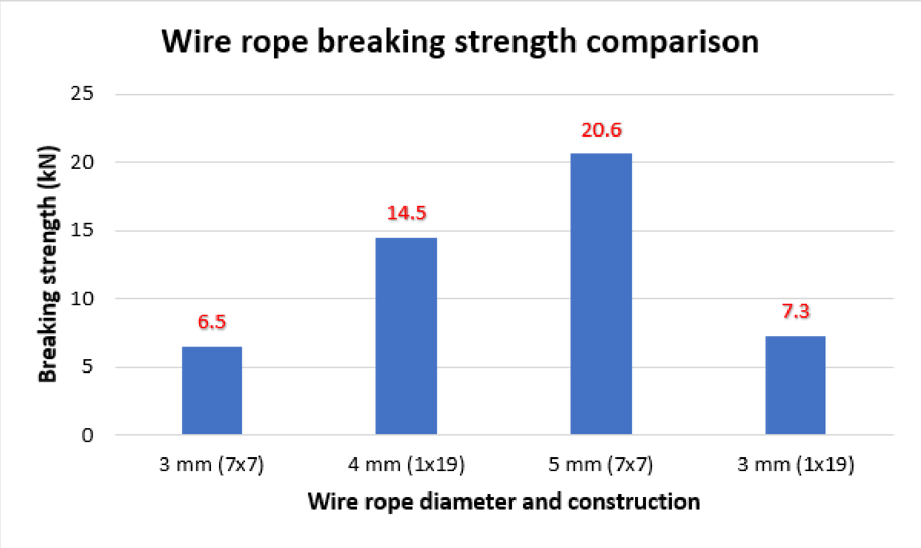

Figure 31: Breaking strength as a function of wire rope diameter and strand construction

From Figure 31, the breaking strength of the of the 3 mm diameter (7x7) wire rope was 6.5 kN, while the 4 mm (1x19) wire rope had a breaking strength of 14.5 kN. The 5 mm (7x7) and 3 mm (1x19) wire ropes had breaking strengths of 20.6 kN and 7.3 kN. Due to its construction, the 1x19 wire ropes also had a marginally higher breaking strength than the 7x7 wire ropes of the same diameter. This difference in breaking strength could potentially be attributed to the larger diameter individual wires used in the construction of the 1x19 wire ropes. The wire rope construction is the arrangement of the steel wires braided around a central steel wire core (Figure 21). Larger diameter individual wires have higher breaking strength and bending stiffness. However, challenges may arise in the weaving process of the inner and perimeter wire ropes during the production of wire rope mesh if the wire ropes have high bending stiffness.

From Figure 31 it is evident that the breaking strength of the 4 mm (1x19) wire rope is 123% higher than the 3 mm (7x7) wire rope. The 4 mm (1x19) wire rope could thus be used as a substitute for the 3 mm (7x7) wire rope. Although the breaking strength of the 4 mm (1x19) wire rope is 42% lower than that of the 5 mm (7x7) wire rope, it may still be a potential substitute for the 5 mm wire rope. Conducting tests on the 4 mm wire rope to demonstrate its suitability as an alternative to both the 3 mm and 5 mm wire ropes will allow MSP to mitigate the risk of potential supply issues of the 3 mm and 5 mm wire ropes in the future.

From Figure 32 the 4 mm (1x19) wire rope had the highest ultimate tensile strength of 1153 MPa. The 3 mm (1x19) and 5 mm (7x7) wire ropes had similar tensile strength of 1057 MPa and 1043 MPa respectively. The 3 mm (7x7) wire rope had the lowest tensile strength of 909 MPa. A slight slippage of the 5 mm (7x7) wire rope occurred in the clamping system during testing, resulting in a drop in tensile strength from 150 MPa to 50 MPa at a strain rate of 0.25.

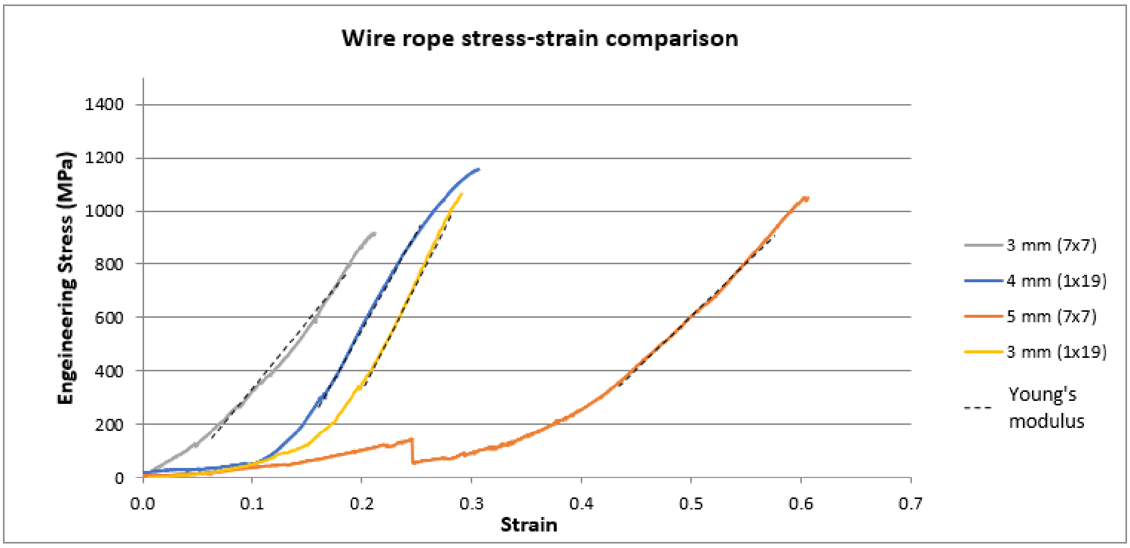

Figure 32: Engineering stress-strain graph of different wire rope diameters and strand constructions

Figure 32 also shows the difference in Young's modulus between the four different wire ropes. The 4 mm (1x19) and 3 mm (1x19) curves had similar gradients, indicating that they have similar Young's modulus. These two curves also had the steepest gradients, suggesting that these wire ropes have higher resistance to elastic deformation than the 3 mm (7x7) and 5 mm (7x7) wire ropes. The 5 mm (1x9) wire rope had the shallowest gradient, which indicates it had the lowest Young's modulus and therefore had the lowest resistance to elastic deformation.

4.3 Drop test

Drop tests were done on four different configurations, as outlined in Table 2 and Section 3.4. A 455 kg weight was used for the drop tests. The first configuration consisted of 3 mm (7x7) inner and 5 mm (7x7) perimeter wire ropes. The second configuration wire mesh was made of 3 mm (7x7) inner and 4 mm (1x19) outer wire ropes. In the third configuration, 4 mm (1x19) were used for both the inner and perimeter wire ropes. 1.5 x 1.5 m mesh sizes were used for the first three configurations. The fourth configuration consisted of two 1.5 x 1.5 m meshes hooked together with six Rocnet connectors to form a 1.5 x 3 m wire mesh modular system. The meshes used for the modular system consisted of 3 mm (7x7) inner and 5 mm (7x7) outer wire ropes. Only one drop test from 100 mm was done on the modular system to assess the feasibility of using six Rocnet connectors per side and to determine the deflection of the modular system. For each configuration, the drop test heights were increased by increments of 100 mm until failure. The results of these drop tests on the four different configuration wire meshes are given in Figure 33.

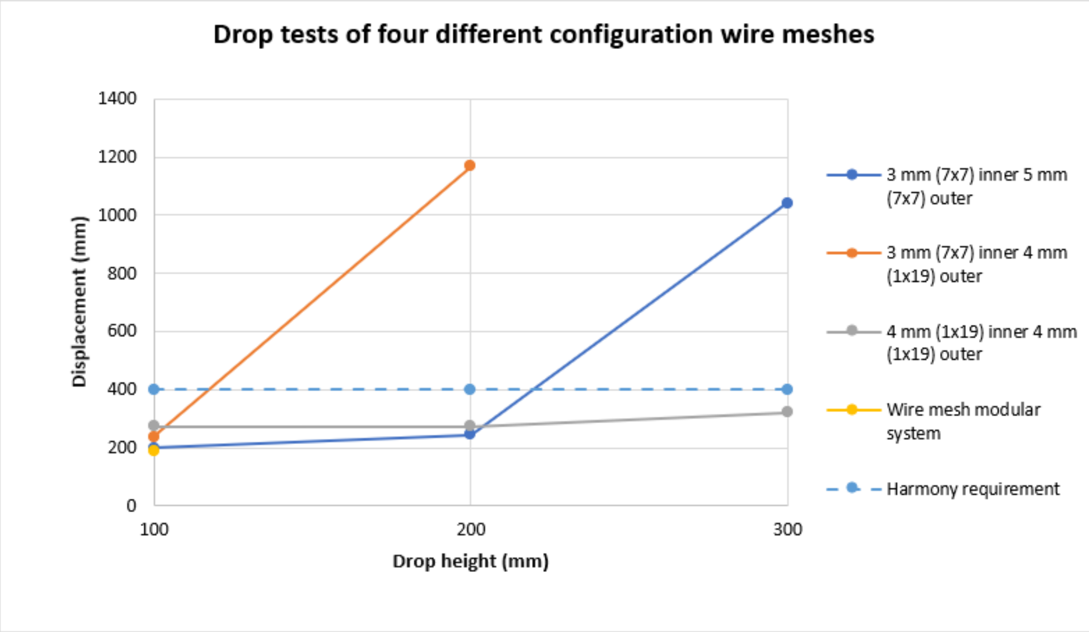

Figure 33: Wire mesh displacement as a function of drop height for different diameter and construction wire ropes

All four configurations performed within the required specification of stopping a 455 kg weight dropped from 100 mm with the wire mesh not deflecting more than 400 mm. The 3 mm (7x7) inner and 5 mm (7x7) perimeter wire rope mesh deflected by 200 mm from a drop test height of 100 mm, as shown in Figure 33. The wire mesh had a maximum deflection of 244 mm from a drop test height of 200 mm, resulting in fracture of the inner wire rope at two attachment points. The attachment points refers to the points at which the wire mesh is attached to the test frame.

Although fracture of the inner wire ropes occurred, the wire mesh deflection was still within the Harmony Gold spec of a maximum deflection of 400 mm. Configuration 1, with 3 mm (7x7) inner and 5 mm (7x7) outer wire ropes, failed at a drop test height of 300 mm. The failure mechanism involved fracture of both the 3 mm (7x7) inner and the 5 mm (7x7) perimeter wire ropes. As a result, the weight fell through the mesh and landed on the ground, exceeding the maximum allowable deflection of 400 mm.

The 3 mm (7x7) inner and 4 mm (1x19) perimeter wire rope mesh failed at a drop test height of 200 mm. Failure also occurred due to ductile fracture of the 3 mm (7x7) inner and 4 mm (1x19) outer wire ropes. The weight thus fell through the mesh and reached the ground, exceeding the maximum allowable deflection of 400 mm. The wire mesh displacement from a drop test height of 100 mm was 237 mm. For the 4 mm (1x19) inner and perimeter wire rope mesh, three drop tests were done with a maximum drop height of 300 mm. Tests were stopped at a drop height of 300 mm due to the mesh still not exceeding the maximum permitted deflection of 400 mm. No fracture of the 4 mm (1x19) inner and perimeter wire ropes was evident. This implies that configuration 3 wire mesh design with 4 mm (1x19) inner and perimeter wire ropes may be an overdesign.

For the wire mesh modular system, drop tests from a height of 100 mm were done on two 1.5 x 1.5 m meshes hooked with six 5 mm spring steel Rocnet connectors to form a wire mesh modular system of 1.5 x 3 m. The meshes were made of 3 mm (7x7) inner cable and 5 mm (7x7) outer cable. From Figure 33 it is evident that the Rocnet modular system deflected 190 mm after a drop test from 100 mm. Fracture of the outer wire rope occurred at one attachment point.

For the 3 mm (7x7) inner and 5 mm (7x7) outer wire rope mesh, fracture of the inner and outer wire ropes occurred after a drop test from a height of 300 mm. This resulted in a displacement exceeding the permissible maximum of 400 mm. A peak force of 69 kN was exerted on the weight when the wire mesh failed and the weight came in contact with the ground as can be seen in Figure 34. The force on the wire mesh from a drop test height of 200 mm was less than from 100 mm. This may be due to fracture of the inner wire rope at two attachment points from a drop test height of 200 mm. The fracture of these two inner wire ropes causes a deceleration of the weight, resulting in reduced force exerted on the wire mesh when it ultimately stops the weight.

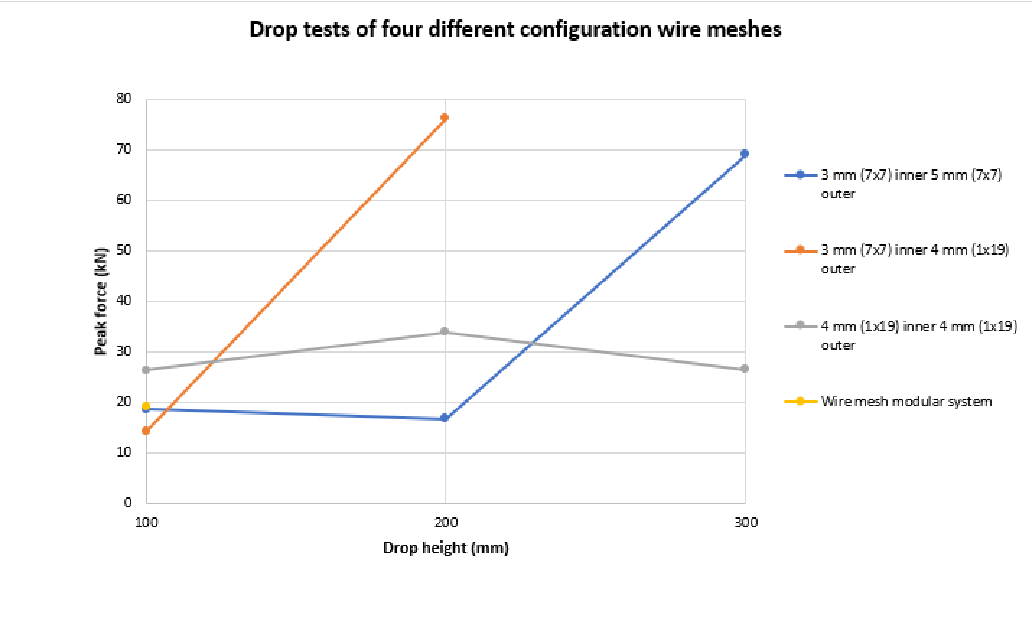

Figure 34: Peak force on wire mesh as a function of drop height for different diameter and construction wire ropes

For the 3 mm (7x7) inner and 4 mm (1x19) outer wire rope mesh, fracture of the 3 mm (7x7) inner and 4 mm (1x19) outer wire ropes occurred after a drop test from a height of 200 mm. Additionally, a peak force of 76 kN was exerted on the weight as it made contact with the ground. In the case of the 4 mm (1x19) inner and outer wire rope mesh, the force applied to the wire mesh increased marginally from 26.3 kN at a drop test height of 100 mm to 27 kN at 300 mm. This slight increase in force is expected as an increase in kinetic energy of the falling weight should result in an increase in force exerted on the wire mesh. For the wire mesh modular system, a force of 19 kN was exerted on MSP's wire mesh modular system from a drop test height of 100 mm. Fracture of the 5 mm (7x7) outer wire rope occurred.

The 3 mm (7x7) inner and 5 mm (7x7) wire rope mesh began to show signs of fracture of the wire ropes from the first test which was from a drop test height of 100 mm, as indicated in Figure 35 (a). Fracture of the 3 mm (7x7) inner wire rope at one attachment point occurred, however the wire mesh still performed within specifications; deflections were less than 400 mm. From a drop height of 200 mm, the 3 mm wire rope fractured at two attachment points but the wire mesh still performed within spec as indicated in Figure 33. Deflection was 44 mm more than the drop test from 100 mm due to the 3 mm wire rope fracture.

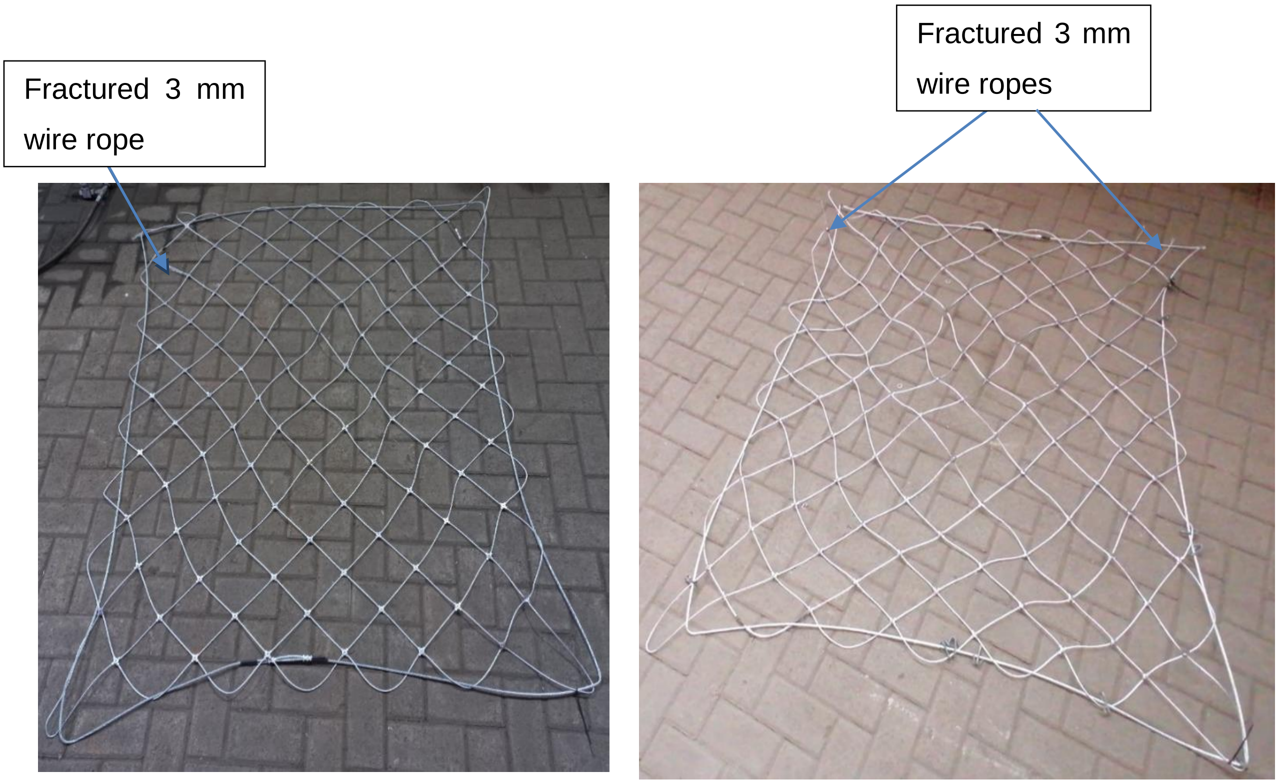

(a) (b)

Figure 35: (a) 3 mm (7x7) inner and 5 mm (7x7) outer wire rope mesh condition after a 100 mm drop test and (b) after a 200 mm drop test

From a drop test height of 300 mm, the 3 mm (7x7) inner wire rope fractured at two attachment points and the 5 mm (7x7) outer fractured at one attachment point which ultimately led to the wire mesh failing, as shown in Figure 36. Ductile fracture occurred in both the inner and outer wire ropes, as indicated in Figure 41, suggesting that the mesh was overloaded. However, the wire mesh still exceeded the specified requirement of not deflecting more than 400 mm from a 100 mm drop, only deflecting 244 mm from a 200 mm drop test. As a result, the 3 mm (7x7) inner and 5 mm (7x7) wire rope mesh met the criteria for underground use as per the Harmony Gold standard.

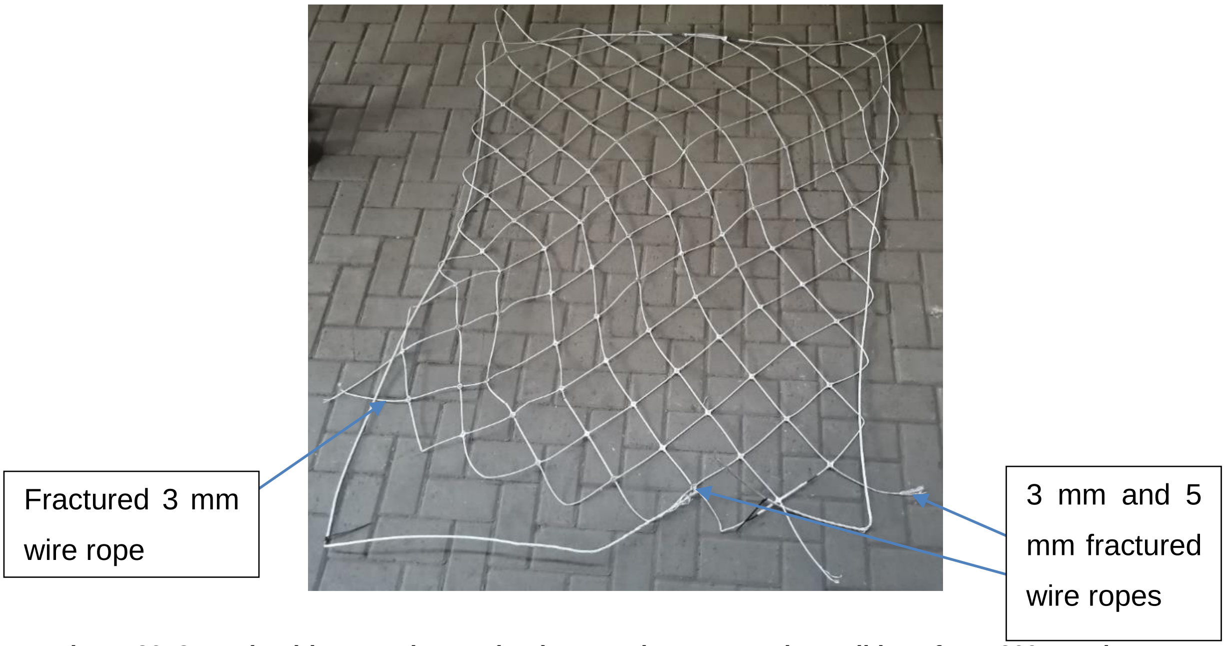

Figure 36: 3 mm (7x7) inner and 5 mm (7x7) outer wire rope mesh condition after a 300 mm drop test

For the 3 mm (7x7) inner and 4 mm (1x19) outer wire rope mesh, fracture of the wire ropes occurred after a drop test from 100 mm, as shown in Figure 37 (a). Fracture of the 3 mm (7x7) inner wire rope occurred at one attachment point with the wire mesh deflecting by 237 mm. From a drop test height of 200 mm, the wire mesh failed due to fracture of the 3 mm wire rope at two attachment points and 4 mm (1x19) wire rope at one attachment point, as indicated in Figure 37 (b). The fracture of both wire ropes was also ductile, as shown in Figure 41.

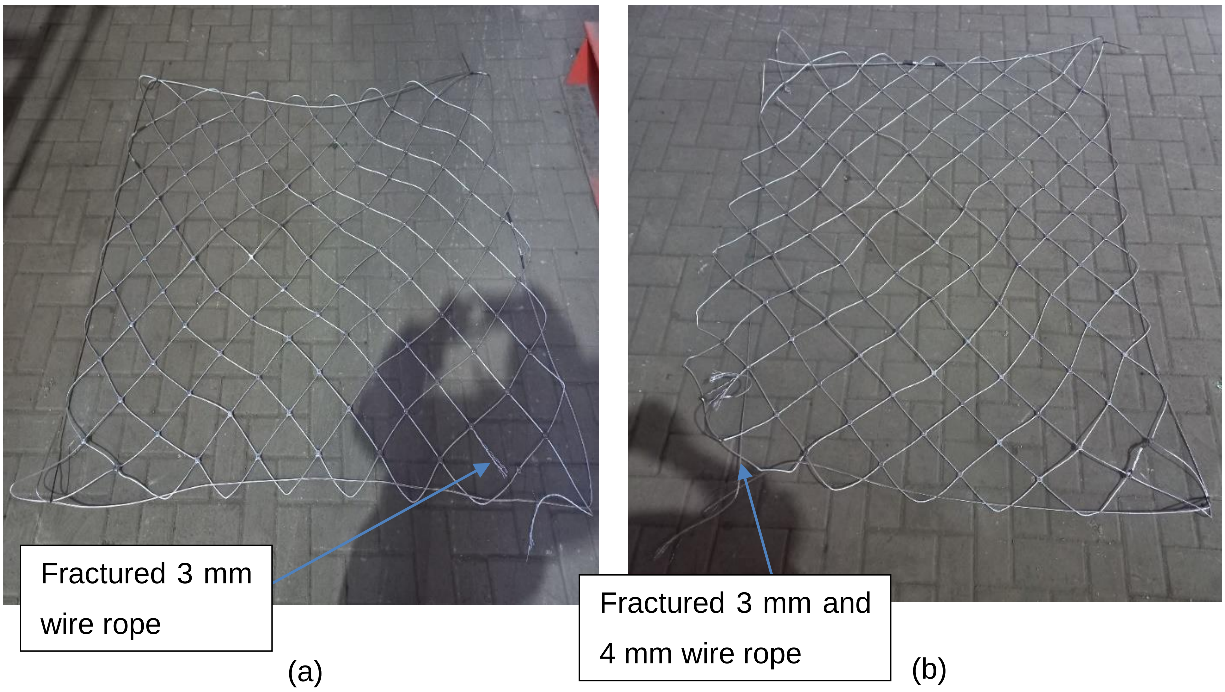

Figure 37: (a) 3 mm (7x7) inner and 4 mm (1x19) outer wire rope mesh condition after a 100 mm drop test and (b) after a 200 mm drop test

The 4 mm (1x19) inner and outer wire rope mesh showed no signs of fracture to any of the wire ropes for drop tests from 100 mm, 200 mm and 300 mm, as indicated in Figure 38 and 39 . The wire mesh performed within specification for all three tests.

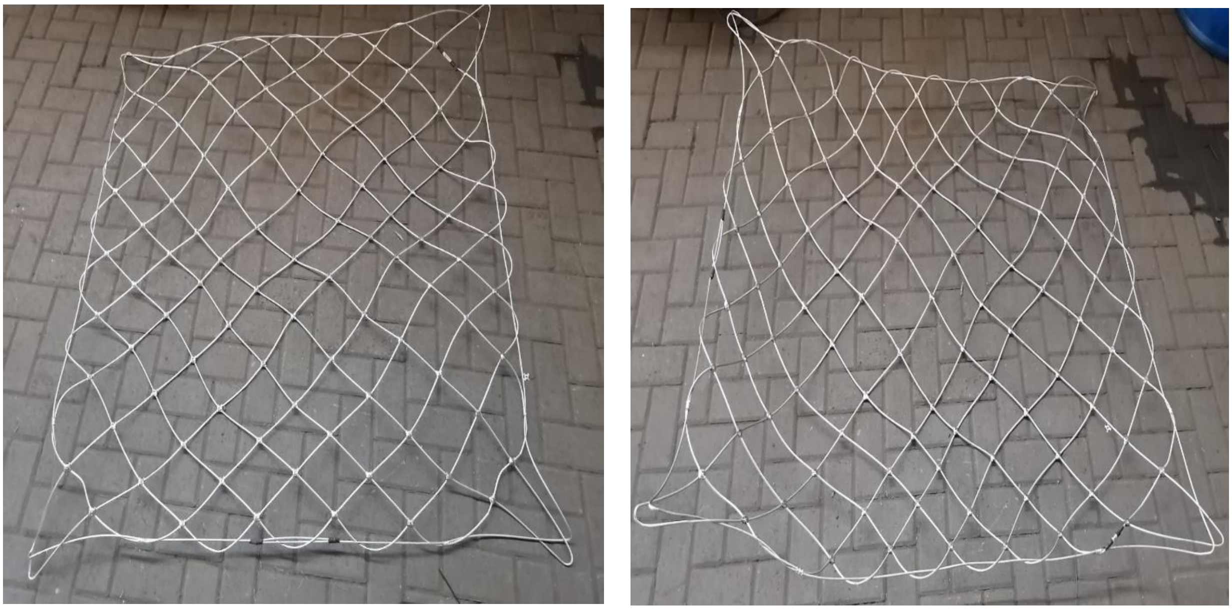

(a) (b)

Figure 38: (a) 4 mm (1x19) inner and outer wire rope mesh condition after a 100 mm drop test and (b) after a 200 mm drop test

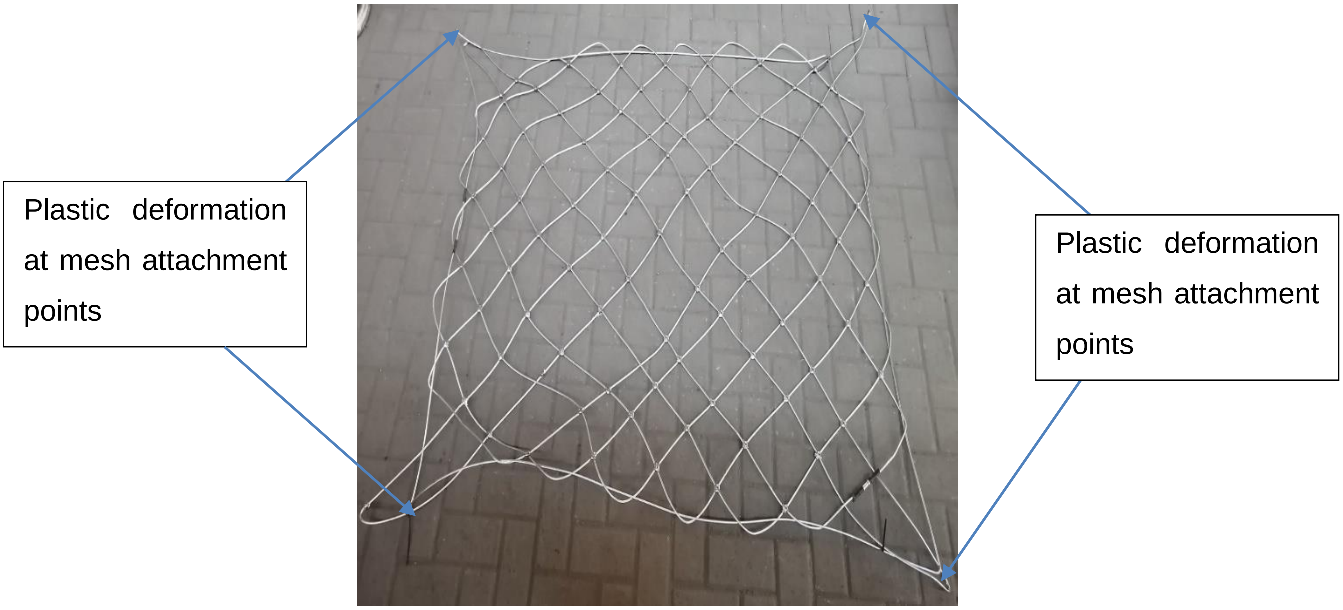

Figure 39: 4 mm (1x19) inner and outer wire rope mesh condition after a 300 mm drop test

For the wire mesh modular system, the weight was dropped at the centre of the mesh and fracture of the 5 mm (7x7) outer wire rope occurred at one attachment point, as indicated in Figure 40. The fracture observed in the outer wire rope also displayed ductile characteristics, as shown in Figure 41.

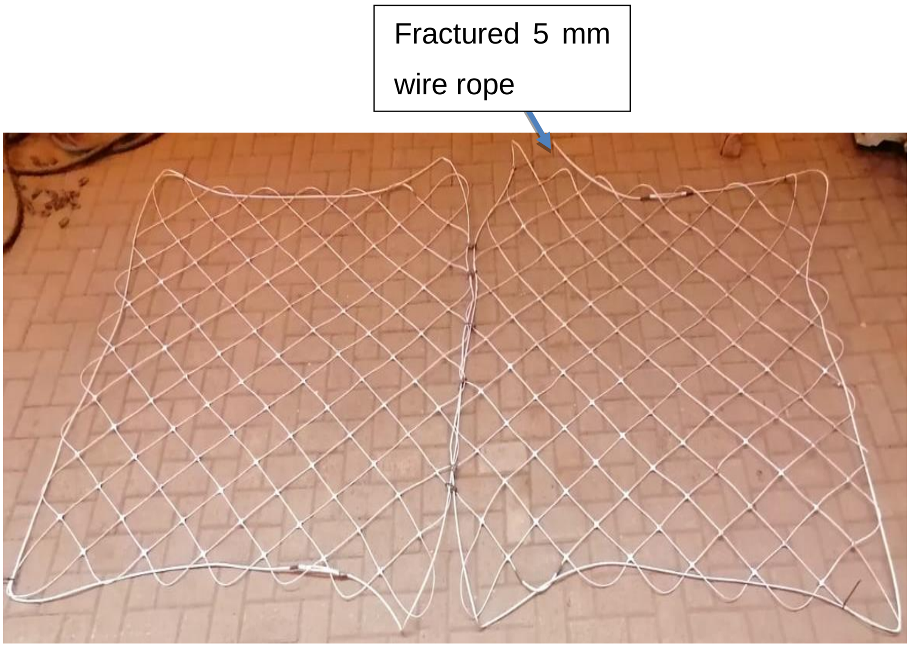

Figure 40: Wire mesh modular system after a 100 mm drop test

Figure 41: Wire rope ductile fracture

No visible plastic deformation of the Rocnet connectors was observed after a drop test from 100 mm on the wire mesh modular system, as illustrated in Figure 42.

Figure 42: Rocnet connectors after drop test

4.4 FEA design

FEA on drop tests on MSP's wire mesh was done on three different configurations as per Table 2. For each configuration, the drop test heights were incrementally raised by 100 mm intervals, and then compared with the corresponding experimental results. The first configuration consisted of 3 mm (7x7) inner and 5 mm (7x7) perimeter wire ropes. The second configuration featured 3 mm (7x7) inner and 4 mm (1x19) outer wire ropes. In the third configuration, 4 mm (1x19) were used for both the inner and perimeter wire ropes. A FEA was done of the drop test on these three configuration wire meshes and compared with experimental results. Results of the first configuration FEA drop test results and comparison with experimental results are given in Figure 43.

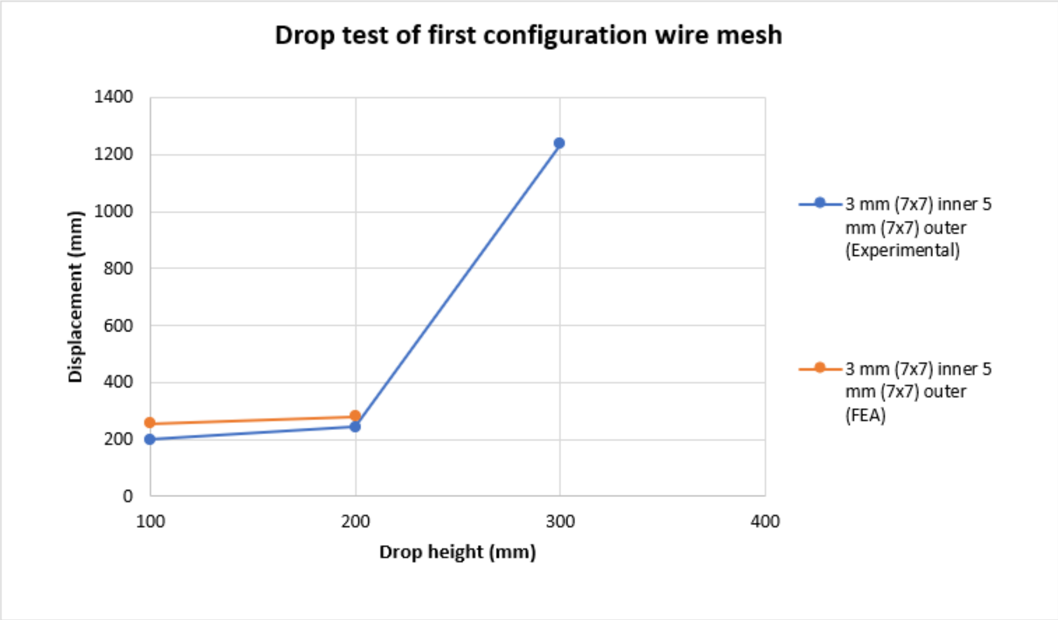

Figure 43: Experimental and FEA displacement as a function of drop height for the first configuration

From Figure 43 it can be seen that the FEA results compared reasonably well with the experimental results. From a drop test height of 100 mm, the wire mesh displacement from the FEA was 18% more than the displacement obtained from the experimental results. From a drop test height of 200 mm the FEA wire mesh displacement was 8.9% more than the experimental displacement. A FEA was only done from 100 mm and 200 mm to compare the deflection with experimental results. Failure of the wire mesh occurred from a drop test height of 300 mm in the experimental test and was therefore not comparable with a FEA drop test from 300 mm.

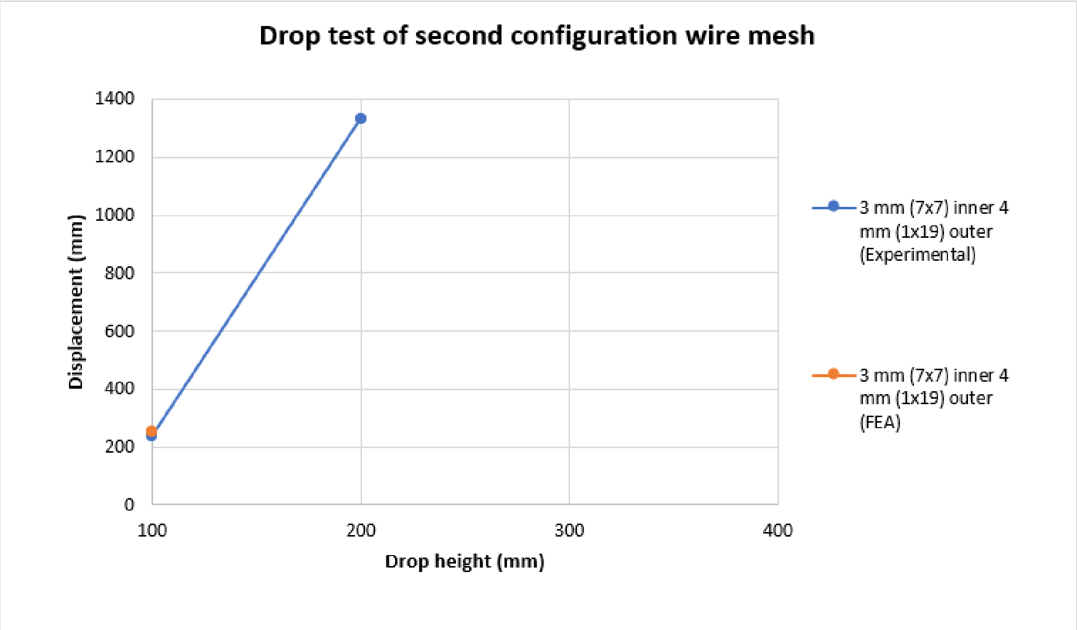

Figure 44: Experimental and FEA displacement as a function of drop height for the second configuration

The FEA wire mesh displacement after a drop test height of 100 mm also showed good correlation with experimental results for configuration 2 wire mesh, as can be seen in Figure 44. The wire mesh displacement of the FEA was 5.6% more than the experimental results. In the experimental results, fracture of the inner and outer wire ropes occurred from a drop test height of 100 mm, leading to failure of the wire mesh. A FEA was thus only done from 100 mm to compare the difference in deflection between the FEA and experimental results. It should be noted that the wire mesh failed from a drop test height of 200 mm in the experimental test, making direct comparison with a FEA drop test at 200 mm unfeasible.

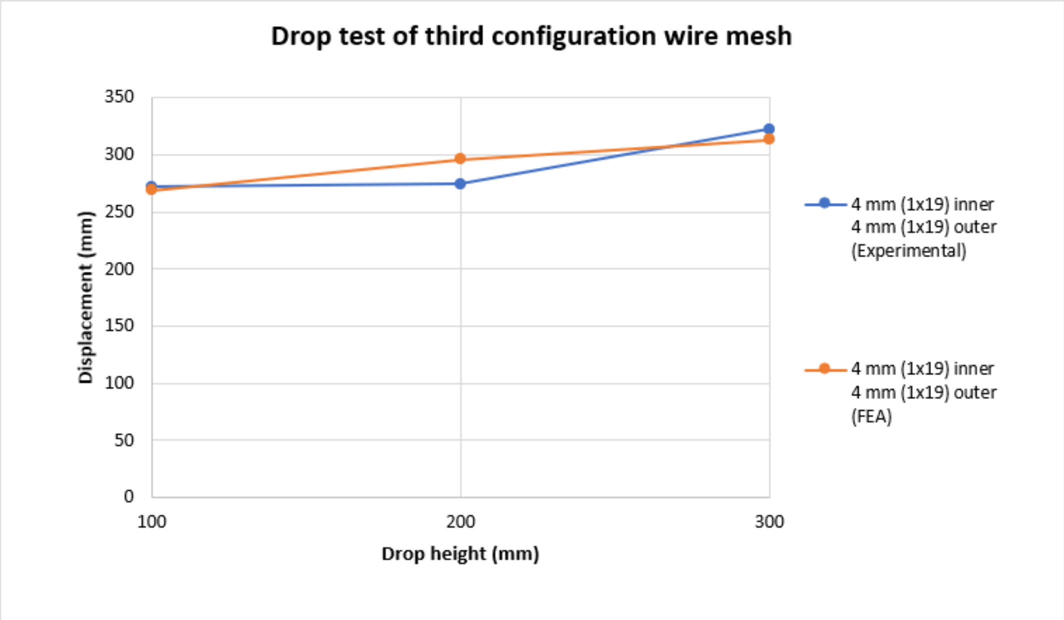

Figure 45: Experimental and FEA displacement as a function of drop height for the third configuration

From Figure 45 it can be seen that the FEA results compared well with the experimental results for configuration 3. From a drop test height of 100 mm, the FEA wire mesh displacement was only 1.1% lower than the experimental results. From a drop test height of 200 mm the FEA displacement was 7.4% higher than experimental results, and from 300 mm, it was 2.8% lower than experimental results.

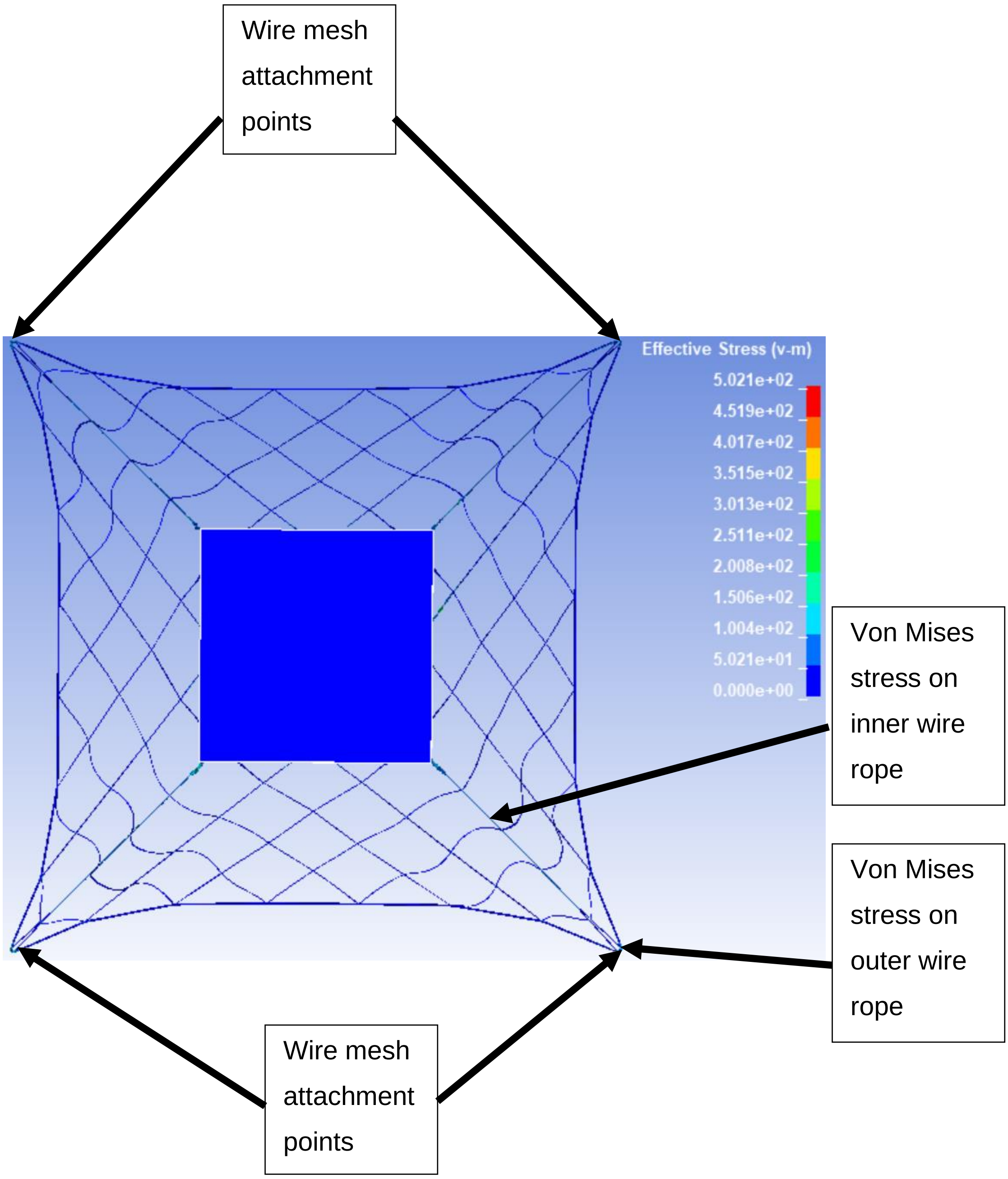

Figure 46: Von Mises stress on MSP's wire mesh during drop test

The von Mises stress distribution on the wire ropes of MSP's wire mesh was also analysed using the FEA, as can be seen in Figure 46. Von Mises stress is commonly used in FEA's to determine if a material will yield. Analysing the stress distribution on certain strands of wire rope may allow for recommendations to further improve MSP's wire mesh.

From Figure 46 it is evident that inner and outer wire rope strands attached to attachment points experience more stress than other strands. This supports the evidence from the experimental tests, where the inner wire ropes fractured first at the attachment points. followed by the outer wire ropes which also fractured at the attachment points.

4.5 Influence of corrosion

Galvanized wire ropes with a 1x19 configuration and a diameter of 3 mm were left underground in a South African gold mine for 76 days, followed by subsequent tensile tests. The breaking strength of the corroded wire ropes was compared with new 3 mm diameter (1x19) wire rope. The results are given in Figure 47.

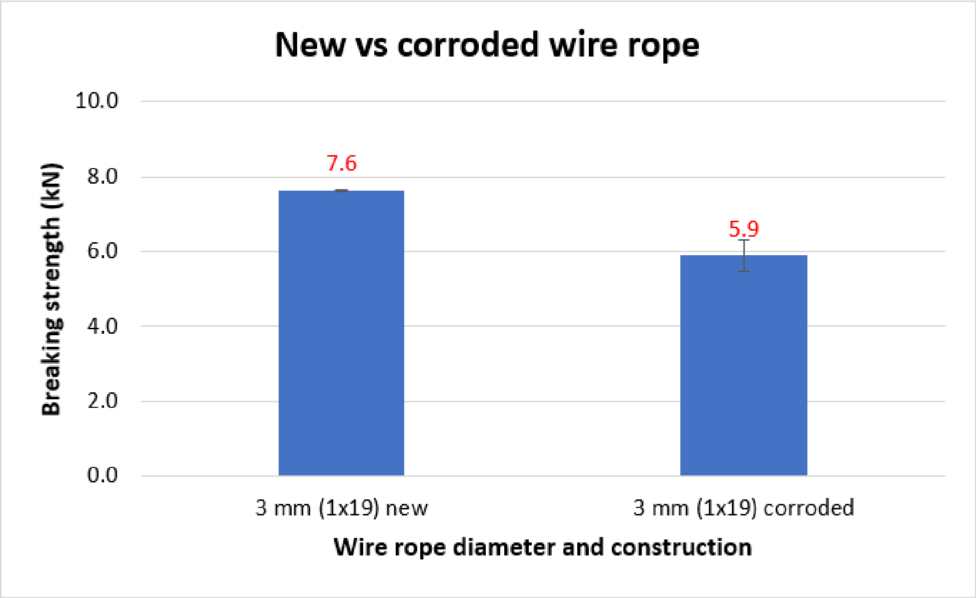

Figure 47: Breaking strength as a function of wire rope diameter and strand construction for new and corroded 3 mm (1x19) wire ropes

Three samples of both the new and corroded wire ropes were tested, and as can be seen from Figure 47, had average breaking strengths of 7.6 kN and 5.9 kN respectively. The decrease in breaking strength between the new wire rope and corroded wire rope equates to 22.5%. This indicates that a corroded wire mesh may fracture and ultimately fail at a lower drop height. From the drop tests it was evident that the performance of the wire mesh is dependent on the breaking strength of the wire ropes. Wire mesh made of wire ropes with higher breaking strength fractured at a higher drop test height. For example, the 4 mm (1x19) inner and perimeter wire rope mesh showed no signs of damage from a drop test height of 300 mm. The 4 mm (1x19) inner wire rope had a breaking strength 123% higher than the 3 mm (1x19) wire rope, which was used for the other three wire mesh configuration.

Figure 48: Galvanized PVC coated wire rope (top), galvanized wire rope (middle) and galvanized wire rope coated with bitumen (bottom) from MSP's wire mesh before salt spray test

Salt spray tests were done on galvanized 3 mm (1x19), PVC and bitumen coated wire ropes. The wire ropes were exposed to 168 hours of testing as per ASTM (2018), the standard practice for operating salt spray (fog) apparatus. Photographs were taken before (Figure 48) and after (Figure 49) salt spray exposure.

Figure 49: Galvanized PVC coated wire rope (top), galvanized wire rope (middle) and galvanized wire rope coated with bitumen (bottom) from MSP's wire mesh after salt spray test

As can be seen from Figure 49, the galvanized PVC coated wire rope had almost no traces of corrosion products. White corrosion products were only evident at the cut ends which were not PVC coated. The galvanized wire rope was completely covered with white and traces of brown corrosion products. White corrosion products forms because of zinc corrosion (Gao *et al*., 2018). The zinc coating is thus penetrated, and the metal underneath corrodes, which is when brown corrosion products form. White corrosion products also formed on the bitumen coated wire rope. Due to the lack of brown corrosion on the bitumen coated wire rope, the metallic body may have been uncorroded after 168 hours of salt spray testing.

4.6 Discussion of results

From the tensile tests done on the 3 mm (7x7), 5 mm (7x7), 4 mm (1x19) and 3 mm (1x19) wire ropes it was evident that breaking strength increased with increasing wire rope diameter, as shown in Figure 31. This observation aligns with findings by Wang *et al*. (2022). Tensile tests of geogrid strands revealed increasing the number of wires in strands resulted in higher breaking strength. Similarly, in welded wire mesh, bigger wire diameters were associated with an increase in individual wire breaking strength.

From the drop test results is evident that all four configurations of MSP's wire mesh performed well within the Harmony Gold spec of not deflecting more than 400 mm after a drop test from 100 mm. For the 3 mm (7x7) inner and 5 mm (7x7) outer wire rope mesh, as well as the 3 mm (7x7) inner and 4 mm (1x19) outer wire rope mesh configurations, fracture of the inner wire ropes occurred first. Observations revealed fracture to the outer wire ropes occurred after fracture of the inner wire ropes. The fractures observed in the 3 mm (7x7), 5 mm (7x7), and 4 mm (1x19) wire ropes had ductile characteristics, as illustrated in Figure 41. The load is therefore distributed from the inner wire ropes, which is the first impact point, to the attachment points. In the case of the wire mesh modular system, fracture of the outer wire rope occurred first. The load was thus distributed from the outer wire rope, which was the first point of impact, to the attachment points. All fractures happened at the attachment points. This observation was also made by Skarbøvig *et al*., (2011). Drop tests were done on a polymer mesh, failure of the mesh also occurred at the attachment points at a kinetic energy of 2.21 kJ, equivalent to a 450 kg weight dropped from a height of 500 mm. In a study done by Morton *et al*. (2007), welded wire mesh failed at the attachment points when subjected to static tests. Weld failure and failure in the HAZ at the attachment points were noted.

From a drop height of 300 mm, the deflection of the 4 mm (1x19) inner and perimeter wire mesh measured 289 mm, which is well within the Harmony Gold requirement of a maximum allowable deflection of 400 mm. There was also no substantial increase in wire mesh deflection with the increase in drop heights, as shown in Figure 33. This could be due to the 1 x 19 wire construction, which has higher resistance to elastic deformation than the other wire ropes. Materials with higher resistance to elastic deformation has a higher Young's modulus (Jones & Ashby, 2019). This increased Young's modulus is evident in Figure 32, where the stress-strain curve of the 4 mm (1x19) wire rope has a steeper gradient in the elastic region than that of the 3 mm (7x7) and 5 mm (7x7) wire ropes. The elastic region of the stress-strain graph corresponds to the section before plastic deformation occurs as indicated in Figure 32.

Unlike the other 2 configurations, the 5 mm (7x7) outer wire rope of the wire mesh modular system fractured first with no fracture of the inner wire rope (Figure 40). This may be because the first impact point was on the outer wire ropes. From figures 37 to 42 it is evident that plastic deformation of the wire meshes occurred at the attachment points for all four configurations. This plastic deformation was localized, with deformation of the wire ropes only visible at the mesh attachment points. No visible plastic deformation occurred at the centre of the meshes. Fracture of the 5 mm (7x7)) wire rope was also ductile in nature as can be seen in Figure 41. This observation suggests the wire meshes were overloaded. Static and dynamic tests of welded wire mesh also revealed ductile fracture of steel wires (Player *et al*., 2008).

The 4 mm (1x19) inner and outer wire rope mesh was the only design that did not show any signs of wire rope fracture even after a drop test height of 300 mm. This may be due to the 4 mm (1x19) having a breaking strength 123 % higher than the 3 mm (7x7) wire rope which was used for the inner wire rope for the other configurations (Figure 31). Wire breaking strength can significantly influence the mesh performance (Wang *et al*., 2022). Geogrid strands with breaking strengths of 7.88 kN and 12.67 kN were weaved into a geogrid mesh pattern and static tests of the geogrid mesh indicated that the breaking strength of the mesh was 53 kN and 91.76 kN respectively. Similarly, welded wire mesh, comprising wires with breaking strengths of 8.53 kN and 33.17 kN, underwent static testing, revealing breaking strengths for the welded wire mesh at 34.3 kN and 45.52 kN. Schoevaerts *et al*. (2012) also conducted a study comparing static tests of chain link mesh using high tensile wire with breaking strengths of 12 kN and 22 kN. The results of the static tests indicated that the chain link mesh with the two different wires, had breaking strengths of 50 kN and 110 kN, respectively. This relation between higher wire rope breaking strength and improved mesh performance can also be seen with the 3 mm (7x7) inner and 5 mm (7x7) outer wire rope mesh and 3 mm (7x7) inner and 4 mm (1x19) outer wire rope mesh. The only difference between the two meshes is the 5 mm (7x7) and 4 mm (1x19) outer wire ropes. The 5 mm (7x7) wire rope had a breaking strength 42 % higher than the 4 mm (7x7). As a result configuration 1 wire mesh, with 3 mm (7x7) inner and 5 mm (7x7) outer wire ropes, failed after a drop height of 300 mm. Configuration 2 wire mesh, with 3 mm (7x7) inner and 4 mm (1x19) outer wire rope, failed at 200 mm.

Using six spring steel Rocnet connectors with diameter of 5 mm each was found to be adequate for the wire mesh modular system, as indicated in Figure 40. Less than six Rocnet connectors may be used due to no visible deformation of the connectors after testing. However, six Rocnet connectors resulted in a connector at each loop of the mesh, excluding the attachment points to the frame. A connector at each loop may simplify underground installations. Due to similar pricing and better availability, 5 mm diameter spring steel was selected over the 4 mm diameter option. All four tested configurations of MSP's wire mesh therefore comply with the Harmony Gold technical specifications for safety nets used in development and stope faces.

A good correlation between the FEA and experimental wire deflections was evident. The differences in FEA and experimental wire mesh displacements ranged from 1.1% to 18%. These results shows a good correlation, aligning well with findings from Morton *et al*. (2007) and Wang *et al*. (2021). Morton *et al*. (2007) achieved a maximum accuracy of 7%, while Wang *et al*. (2021) achieved 18%.

Von Mises stress distribution on MSP's wire mesh was also analysed using the FEA, as illustrated in Figure 46. It was evident that the inner and outer wire ropes connected to the attachment points experienced more stress than other strands. This supports the evidence from the experimental tests, where the inner wire ropes fractured first at the attachment points. Subsequently, the outer wire ropes attached to these points also fractured, resulting in the failure of the wire mesh.

The corrosion observed on the galvanized wire ropes that were placed underground in a gold mine for a duration of 76 days, resulted in a notable 22.5% reduction in tensile strength as shown in Figure 47. This reduction in tensile strength may be due to the decrease in wire rope diameter caused by corrosion, which may be attributable to the high levels of humidity and temperature experienced in the environment. The temperature and relative humidity levels recorded in the South African gold mine, where the galvanized wire ropes underwent corrosion, were 30°C and 95% respectively (Table 4). Corrosion rates of galvanized wire ropes have been found to increase linearly from 10°C to 40°C (Suzumura & Nakamura, 2004). Corrosion rates have also been found to increase above a relative humidity of 60% (Dorion *et al*., 2009). Contamination of groundwater may also have had an influence on the corrosion of the galvanized wire rope. The wire ropes may be exposed to groundwater due to the high pressure water jets used to collect broken ore. Aggressive ions such as Cl and SO_4 ions were found in the groundwater in the area where the galvanized wire ropes were placed. These ions in water attack the thin protective film on metals, therefore making the metal more prone to corrosion (Hadjigeorgiou *et al*., 2008). Similarly, Song et al. (2017) noted a trend where higher Cl concentrations were associated with higher corrosion rates of carbon steel.

PVC coating had a noticeable effect on the corrosion of the galvanized wire ropes, with white corrosion products only formed on the cut ends of the wire ropes. This corrosion protection provided by PVC coatings can be attributed to the additional barrier protection it provides, as was also observed by Bandeira *et al*. (2017). The costs of PVC coated wire ropes also compared well with uncoated galvanized wire ropes and remained largely unaffected by the salt spray test, as shown in Figure 49. However, using aluminium ferrules on PVC coated wire ropes may cause slippage of the wire ropes. Ferrules are used to connect the two endpoints of wire ropes and are therefore an important part of the wire rope mesh. More tests are needed to verify the performance of aluminium ferrules swaged on PVC coated wire ropes.

Similarly, bitumen coating also had a noticeable effect on corrosion of the galvanized wire ropes in which only white corrosion products was evident. In comparison, brown corrosion products were also evident on uncoated galvanized wire ropes. Although bitumen does not possess corrosion inhibiting properties, it provides a protective layer that prevents corrosion agents such as oxygen and water from reaching the metal surface (Guma *et al*., 2015). Opting for bitumen to coat MSP’s wire mesh is the most practical option among the three, as an improvement in corrosion resistance was evident when compared to normal galvanized wire rope. Bitumen coating can also be incorporated into the production process and does not affect the performance of the wire mesh.

CHAPTER 6 CONCLUSION AND RECOMMENDATIONS

5.1 Conclusions

The aim of this dissertation was to study the behaviour of MSP's wire mesh when subjected to an impact load. The first objective was to determine and compare the resistance of different configurations of MSP's wire mesh to impact loading using the drop test. Four different configuration wire meshes were chosen and drop tests were done at MSP's test facility.

MSP wire meshes exhibited high impact resistance of stopping a 455 kg weight dropped from 100 mm with the wire meshes not deflecting more than 400 mm. As a result, the wire meshes from MSP are therefore suitable for use as roof support in underground mines. The highest resistance was observed on the mesh with 4 mm (1x19) inner and outer wire ropes.

The second objective was to do a FEA of drop tests on the wire meshes and compare the results with experimental results. The wire mesh displacement was obtained from the FEA and showed good correlation when compared to experimental results. The wire mesh displacement from the FEA ranged from 1.1% to 18% in comparison to experimental results.

The third objective was to determine the influence of corrosion on MSP's wire mesh. Salt spray test were done to determine the influence of corrosion on wire ropes used to manufacture MSP's wire rope mesh. Galvanized wire ropes showed signs of brown corrosion products, bitumen coated wire ropes were less affected and only showed signs of white corrosion products. The bitumen coated wire ropes used to manufacture MSP's wire rope mesh therefore had improved corrosion resistance compared to uncoated galvanized wire ropes. The influence of corrosion was also investigated by leaving galvanized wire ropes to corrode in underground mining conditions. Afterwards, the corroded wire ropes underwent tensile testing to determine its breaking strength and compare it with that of uncorroded galvanized wire ropes. The breaking strength of corroded wire ropes was 22.5% less than that of the uncorroded counterparts. Underground mining conditions therefore had a noticeable effect on the corrosion of galvanized wire ropes.

5.2 Recommendations for future studies

The following recommendations can be made for further studies:

- Determining the resistance of MSP’s wire mesh to impact loading from rockfalls by testing it in situ.
- Conduct drop tests on wire meshes with different widths to determine the influence of wire mesh width on its deflection.
- Conduct drop tests on wire meshes with different aperture sizes to determine its influence on wire mesh performance.
- Conduct FEA of drop tests on MSP’s wire meshes using different software to determine if the accuracy of the deflection obtained from FEA can be improved.
- Conduct FEA of drop tests on MSP’s wire meshes using different software to determine if fracture of the wire mesh can be accurately simulated.
- Testing the influence of corrosion on bitumen and PVC coated wire ropes in an underground environment and compare it with corroded galvanized wire ropes.
- Conduct experimental drop tests on corroded wire meshes made of galvanized wire rope, bitumen coated wire rope and PVC coated wire rope and compare the results with uncorroded wire meshes.
- Analysis of the influence of corrosion on the aluminium ferrules used on MSP’s wire mesh.

BIBLIOGRAPHY

Adedayo, S. & Momoh, S. 2010. Effect of initial elevated metal temperature on mechanical properties of an arc–welded mild steel plate. *Indian Journal of Science and Technology*, 3(12):1224-1228.

ASTM International. 2018. *Operating Salt Spray (Fog) Apparatus.* (ASTM B117-18).

Baboian, R. 2005. *Corrosion tests and standards: Application and interpretation.* 20th ed. ASTM International.

Bandeira, R.M., van Drunen, J., Tremiliosi-Filho, G., dos Santos Junior, J.R. & de Matos, J.M.E. 2017. Polyaniline/polyvinyl chloride blended coatings for the corrosion protection of carbon steel. *Progress in Organic Coatings*, 106:50-59.

Barczak, T.M. 2005. *An overview of standing roof support practices and developments in the United States.* 3rd Southern African Rock Engineering Symposium, Johannesburg, South Africa. pp. 301-334.

Bateman, M., Howard, I., Johnson, A. & Walton, J., 2000. Computer simulation of the impact performance of a wire rope safety fence. *International Journal of Impact Engineering,* 25(1):58-67.

Bright, G., Kennedy, J., Robinson, F., Evans, M., Whittaker, M., Sullivan, J. & Gao, Y. 2011. Variability in the mechanical properties and processing conditions of a high strength low alloy steel. *Procedia engineering*, 10:106-111.

Brownlie, F., Hodgkiess, T., Pearson, A. & Galloway, A. 2022. Electrochemical evaluation of the effect of different NaCl concentrations on low alloy- and stainless steels under corrosion and erosion-corrosion conditions. *Corrosion and Materials Degradation*, 3(1):101-126.

Burstein, G., Liu, C., Souto, R. & Vines, S. 2004. Origins of pitting corrosion. *Corrosion Engineering, Science and Technology*, 39(1):25-30.

Chen, H., Ramandi, H.L., Craig, P., Crosky, A. & Saydam, S. 2022. Stress corrosion cracking of cable bolts in tunnels: An in-situ testing approach. *Tunnelling and Underground Space Technology*, 123:1-16.

Cirak, B. & Kozan, R. 2009. Prediction of the coating thickness of wire coating extrusion processes using artificial neural network (ANN). *Modern Applied Science,* 3(7):52-66.

Cui, L., Wang, M. & Yu, T., 2018. Dynamic Finite Element Analysis of a New Type Flexible Rock Shed under the Impact of Rock Block and Improving the Design, *Shock and Vibration,* 2018*:*1-16.

de la Fuente, D., Castaño, J.G. & Morcillo, M. 2007. Long-term atmospheric corrosion of zinc. *Corrosion Science*, 49(3):1420-1436.

Department of Mineral Resources (South Africa). 2018. Broad-Based Socio-Economic Empowerment Charter for the Mining and Minerals Industry. *Government Gazette,* 41934, 27 Sept.

Dolinar, D. R., 2006. *Load capacity and stiffness characteristics of screen material used for surface control in underground coal mines.* 25th International Conference on Ground Control in Mining (2006), Pittsburgh, USA. pp. 152-158.

Dorion, J. F. & Hadjigeorgiou, J., 2013. *Corrosion considerations in the design and operation of rock support systems.* The Seventh International Symposium on Ground Support in Mining and Underground Construction (2013), Perth, Australia. pp. 497-511.

Du, Y., Peng, J., Richard Liew, J.Y. & Li, G. 2018. Mechanical properties of high tensile steel cables at elevated temperatures. *Construction and Building Materials*, 182:52-65.

Dubina, D., 2004. Ductility and seismic performance of thin-walled cold-formed steel structures. *International Journal of Steel Structures*, 4(4):207-222.

Duffy, J.D. 1992. Flexible wire rope rockfall nets. *Transportation Research Record,* 30-35.

v.d. Westhuizen, E. 2020. Mine Support Products Quotation, September 2020, Vereeniging. (Unpublished quotation).

Fayyad, E.M., Sliem, M.H., Al-Qahtani, N., P. Ryan, M. & Abdullah, A.M. 2024. Assessing underdeposit corrosion inhibitor performance for carbon steel in CO_2/sulfide environment. *Journal of Materials Research and Technology*, 28(4):1433-1451.

Fortes, J.C., Castilla-Gutierrrez, J., Sarmiento, A. & Grande, J.A. 2022. Corrosion of carbon steel in extreme environments by acid mine water: Experimental study of the process using a factorial analysis tool. *Minerals*, 12(8):1030.

Gao, B., Liyang, D., Guanglin, Z., Chao, G. & Ganfeng, T. 2018. Effect of corrosion inhibitors on chromate-free passivation of hot-dip galvanized steel. *Materials Science*, 24(3):265-270

Guma, T., Aku, S., Yawas, D. & Dauda, M. 2015. Bitumen in coating corrosion protection of steel-the position and prognosis of nigerian bitumen. *American Journal Engineering Research*, 4(12):101-111.

Guo, G., Finkenstadt, V.L. & Nimmagadda, Y. 2019. Mechanical properties and water absorption behavior of injection-molded wood fiber/carbon fiber high-density polyethylene hybrid composites. *Advanced Composites and Hybrid Materials*, 2(4):690-700.

Grishanov, S. 2011. 2 - Structure and properties of textile materials. In: Clark, M., eds. *Handbook of Textile and Industrial Dyeing.* Woodhead Publishing. pp. 28-63.

Hadjigeorgiou, J., Dorion, J. & Ghali, E. 2008. Support system performance under different corrosion conditions. *Journal of the Southern African Institute of Mining and Metallurgy,* 108(6):359-365.

Harmony Gold. 2016. *Technical specifications for safety nets used in development and stope faces.* South Africa.

Harmony Gold. 2020. *Standard task procedure for temporary and permanent netting installation.* South Africa.

Harmony Gold 2023. Short form: Results for the six-month period ended 31 december 2022. https://www.harmony.co.za
Date of access: March 2023.

Hayes, H. 1940. Service life of coal-tar enamel protective coatings. *Journal (American Water Works Association)*, 32(10):1705-1722.

Huang, K., Peng, Y., Dong, Y., Chang, X., Zhou, Z., Lu, H., ... Zhang, Q. 2023. Friction and wear behavior of multiple steel wires with different corrosion extents under different lubrication conditions. *Wear*, 524:1-19

Iatan, E. 2021. Chapter 16 - gold mining industry influence on the environment and possible phytoremediation applications. In: Bauddh, K., Korstad, J. & Sharma, P., eds. *Phytorestoration of abandoned mining and oil drilling sites*: Elsevier. pp. 373-408.

Iramina, W. S., Eston, S. M., Hennies, W. T. & Candia, R. C., 2012. *Fatal Accidents and Rockfalls in Peruvian Underground Mines.* Mine Planning and Equipment Selection (2014), Switzerland, Springer International Publishing. pp. 601-609

ISO. 2019. *Metallic materials - Tensile testing - Part 1: Method of test at room temperature.* (ISO 6892-1)

Jackson, K.E., Annett, M.S., Fasanella, E.L. & Polanco, M.A. 2012. *Material model evaluation of a composite honeycomb energy absorber.* 12th international LS-DYNA users conference, Dearborn, United States. pp. 1-21.

Jones, D.R.H. & Ashby, M.F. 2019. Chapter 3 - Elastic Moduli. *Engineering Materials 1 (Fifth Edition).* Butterworth-Heinemann. pp. 31-47.

Keran, Z., Mihaljević, M., Runje, B. & Markučič, D. 2017. Ultrasonic testing of grain distortion direction in cold formed aluminium profile. *Archives of Civil and Mechanical Engineering,* 17(2):375-381.

Minerals Council South Africa. 2019. *Safety in mining fact sheet.*
https://www.mineralscouncil.org.za
Date of access: 11 October 2021

Miyachi, K., Nakamura, S. & Suzumura, K. 2013. Corrosion resistance of steel bridge wires coated with aluminium-zinc alloy. *Bridge Structures*, 69(3):429-438.

Morton, E. C., Thomson, A. G., Villaescusa, E. & Roth, A., 2007. *Testing and analysis of steel wire mesh for mining applications of rock surface support.* ISRM Congress (2014), Lisbon. pp. 1-5

Ortlepp, W.D. & Stacey, T.R. 1997. *Testing of tunnel support: Dynamic load testing of rock support containment systems (eg wire mesh).* Safety in Mines Research Advisory Committee. pp. 1-107.

Player, J. R., Morton, E. & Villaescusa, E., 2008. *Static and dynamic testing of steel wire mesh for mining applications of rock surface support.* 6th International Symposium On Ground Support in Mining and Civil Engineering Construction (2008), Cape Town, South Africa. pp. 693-706.

Potvin, Y. & Heal, D. 2010. *Dynamic testing of high energy absorption (hea) mesh.* Paper presented at the Deep Mining 2010: Proceedings of the Fifth International Seminar on Deep and High Stress Mining, Santiago. pp. 283-300.

Prawoto, Y. & Mazlan, R.B. 2012. Wire ropes: Computational, mechanical, and metallurgical properties under tension loading. *Computational Materials Science*, 56:174-178.

Saville, B.P. 1999. 5 - Strength and elongation tests. *Physical testing of textiles*: Woodhead Publishing. pp. 115-167.

Schoevaerts, B., Balg, C., Brown, S. & Van Zyl, C. 2012. Fast, safe, and fully mechanized installation of high-tensile chain-link mesh for underground support. *Journal of the Southern African Institute of Mining and Metallurgy*, 112(2):127-133.

Singh, R., Mallick, M. & Verma, M., 2016. Studies on failure behaviour of wire rope used in underground coal mines. *Engineering Failure Analysis,* 70:290-304.

Song, Y., Jiang, G., Chen, Y., Zhao, P. & Tian, Y. 2017. Effects of chloride ions on corrosion of ductile iron and carbon steel in soil environments. Scientific Reports, 7(1):1-13.

Sunkpal, M., Roghanchi, P. & Kocsis, K.C. 2018. A method to protect mine workers in hot and humid environments. *Safety and Health at Work*, 9(2):149-158.

Suzumura, K. & Nakamura, S. 2004. Environmental factors affecting corrosion of galvanized steel wires. *Journal of materials in civil engineering*, 16(1):1-7.

Tran, P., Maegawa, K. & Fukada, S. 2013. Experiments and dynamic finite element analysis of a wire-rope rockfall protective fence. *Rock Mechanics and Rock Engineering*, 46(5): 1-24.

Van der Merwe, J. N., van Vuuren, J., Butcher, R. & Canbulat, I., 2001. *Causes of Falls of Roof in South African Collieries,* Safety in Mines Research Advisory Committee. pp. 1-124.

Volkwein, A. 2009. *Numerical modelling of flexible rockfall protection systems.* EGU General Assembly Conference Abstracts. pp. 1-11.

Wang, C., Shankar, K. & Fien, A., 2015. *Finite element simulation of impact response of wire mesh screens.* The European Physical Journal Conferences (2015), Canberra, Australia, EDP Sciences, pp. 1-6.

Wang, C., Wang, H., Shankar, K., Morozov, E. & Hazell, P., 2020. On the mechanical behaviour of steel wire mesh subjected to low-velocity impact. *Thin-Walled Structures,* 159:1-17.

Whiting, R., 2017. *In situ static performance assessment of mine mesh.* 8th International Conference on Deep and High Stress Mining, Australian Centre for Geomechanics, Perth, pp. 747-762.

Wu, J. 2018. Chapter 5 - Material interface of pantograph and contact line. In: Wu, J., ed. *Pantograph and contact line system*: Academic Press. pp. 165-191.

Yang, Y., Yuan, X., Li, Y., He, Z., Zhang, S. & Zheng, S. 2022. Effect of time-varying corrosion on the low-cycle fatigue mechanical properties of wire rope. *Ocean Engineering*, 250: 1-15.

Yu, T. & Xue, P. 2022. *Chapter 4 - Yield criteria. Introduction to engineering plasticity*. Elsevier. pp. 67-87.

Zhang, D., Feng, C., Chen, K., Wang, D. & Ni, X. 2017. Effect of broken wire on bending fatigue characteristics of wire ropes. *International Journal of Fatigue*, 103:456-465.

Zhao, Y., Su, B., Fan, X., Yuan, Y. & Zhu, Y. 2023. Corrosion fatigue degradation characteristics of galvanized and galfan high-strength steel wire. *Materials*, 16 (2):1-23.

Zhu, S., Wu, S., Cheng, J., Li, S. & Li, M. 2015. An underground air-route temperature prediction model for ultra-deep coal mines. *Minerals*, 5(3):527-545.